

Global Analysis of the Relationship between JIL-1 Kinase and Transcription

Catherine Regnard, Tobias Straub, Angelika Mitterweger, Ina K. Dahlsveen, Viola Fabian, Peter B. Becker*

Adolf-Butenandt-Institute and Centre for Integrated Protein Science (CIPSM), Ludwig-Maximilians-University, Munich, Germany

Abstract

The ubiquitous tandem kinase JIL-1 is essential for *Drosophila* development. Its role in defining decondensed domains of larval polytene chromosomes is well established, but its involvement in transcription regulation has remained controversial. For a first comprehensive molecular characterisation of JIL-1, we generated a high-resolution, chromosome-wide interaction profile of the kinase in *Drosophila* cells and determined its role in transcription. JIL-1 binds active genes along their entire length. The presence of the kinase is not proportional to average transcription levels or polymerase density. Comparison of JIL-1 association with elongating RNA polymerase and a variety of histone modifications suggests two distinct targeting principles. A basal level of JIL-1 binding can be defined that correlates best with the methylation of histone H3 at lysine 36, a mark that is placed co-transcriptionally. The additional acetylation of H4K16 defines a second state characterised by approximately twofold elevated JIL-1 levels, which is particularly prominent on the dosage-compensated male X chromosome. Phosphorylation of the histone H3 N-terminus by JIL-1 *in vitro* is compatible with other tail modifications. *In vivo*, phosphorylation of H3 at serine 10, together with acetylation at lysine 14, creates a composite histone mark that is enriched at JIL-1 binding regions. Its depletion by RNA interference leads to a modest, but significant, decrease of transcription from the male X chromosome. Collectively, the results suggest that JIL-1 participates in a complex histone modification network that characterises active, decondensed chromatin. We hypothesise that one specific role of JIL-1 may be to reinforce, rather than to establish, the status of active chromatin through the phosphorylation of histone H3 at serine 10.

Citation: Regnard C, Straub T, Mitterweger A, Dahlsveen IK, Fabian V, et al. (2011) Global Analysis of the Relationship between JIL-1 Kinase and Transcription. *PLoS Genet* 7(3): e1001327. doi:10.1371/journal.pgen.1001327

Editor: Bas van Steensel, Netherlands Cancer Institute, The Netherlands

Received: July 16, 2010; **Accepted:** February 5, 2011; **Published:** March 10, 2011

Copyright: © 2011 Regnard et al. This is an open-access article distributed under the terms of the Creative Commons Attribution License, which permits unrestricted use, distribution, and reproduction in any medium, provided the original author and source are credited.

Funding: This work has been supported by Grants Be1140/6-1 and SFB-TR5-A1 of the Deutsche Forschungsgemeinschaft to PBB. The funders had no role in study design, data collection and analysis, decision to publish, or preparation of the manuscript.

Competing Interests: The authors have declared that no competing interests exist.

* E-mail: pbecker@med.uni-muenchen.de

Introduction

JIL-1 is a ubiquitously expressed, nuclear tandem kinase of *Drosophila melanogaster* that associates with chromatin at all stages of development. JIL-1 phosphorylates histone H3 in chromatin and the kinase is thought to be responsible for the majority of phosphorylation of histone H3 at serine 10 (H3S10ph) in interphase [1]. At the low level of resolution afforded by staining larval polytene chromosomes JIL-1 is seen to associate with active chromatin such as the decondensed interbands of chromosomes [2]. Ectopic recruitment of JIL-1 to a series of Lac operator repeats by fusion to a lacI DNA binding domain leads to local decondensation of polytene chromatin. This reorganisation of chromatin depends on JIL-1's kinase activity [3]. The essential function of JIL-1 can be explained, at least in part, by the involvement of the kinase in chromosome organisation [4,5], where it plays a role in maintaining the balance between euchromatin and heterochromatin [6–8]. This is supported by the fact that *Su(var)3-1* alleles of the *JIL-1* gene are strong suppressors of position effect variegation, which provides a sensitive assay for heterochromatin propagation [9]. In the absence of JIL-1 the H3K9me2 mark and HP1 are redistributed genome-wide and tend to be enriched on the X chromosome in both males and females [6]. In addition, the lethal loss-of-function

mutation of *JIL-1* is rescued by reduced levels of the H3K9 methyltransferase *Su(var)3-9* but not by reduced levels of the major HP1 isoform HP1a [10] suggesting that the spreading of H3K9me2 might be the cause of the lethality of the JIL-1 mutants. However, reducing the dose of *Su(var)3-7*, another essential component of heterochromatin, also rescues the lethality of the *JIL-1* mutant. In this case the redistribution of H3K9me2 was still observed [11]. *Su(var)3-7* may thus be an essential effector in the pathway of heterochromatin spreading, which is counteracted by JIL-1.

In mammalian cells the H3S10ph mark has been implicated in transcriptional activation, notably in immediate early response to mitogen, stress or steroid hormones, which trigger the transient phosphorylation of H3S10 and H3S28 by the kinases Msk1/2 or PIM-1 (for review see [12]). Whereas some of the inducing effects involve the dissociation of euchromatic HP1 isoforms [13,14], the H3S10ph mark also serves as docking site for 14-3-3 proteins, which in turn recruit additional activating enzymes [13,15,16]. In *D. melanogaster*, the role of JIL-1 and the H3S10ph mark in transcription regulation is less clear. Corces and colleagues reported that upon heat shock gene activation, H3S10 phosphorylation by JIL-1 leads to recruitment of 14-3-3 and of the elongator protein 3 (Elp3) [17] that in turn would trigger the transition of an initiated RNA polymerase II (Pol II) into the elongation mode

Authors Summary

Active chromatin is characterised by a wealth of histone modifications that collectively define a decondensed form of chromatin that is accessible to regulators and more easily transcribed. The kinase JIL-1 associates with active chromatin and contributes to chromatin decondensation by phosphorylation of a key serine residue (S10) on the N-terminus of histone H3. We mapped the binding sites for JIL-1 on chromosomes in cells and found that the enzyme associates all along transcribed genes. A basal level of association can be found at most genes and correlates best with the presence of active chromatin exemplified by methylation of H3K36. A double dose of JIL-1 can be observed at active genes of the hyperactive male X chromosome that also bear an acetylation of histone H4 at lysine 16. Phosphorylation of H3 by JIL-1 creates a mark that characterises active chromatin and could play a role in preventing the formation of repressive chromatin. Surprisingly, depletion of the kinase has clear, but relatively modest, effects on transcription. We hypothesise that JIL-1 may help to reinforce the active state of chromatin that is primarily established by other factors.

[18]. Johansen and co-workers by contrast argued that JIL-1 and JIL-1-dependent Ser10 phosphorylation did not have a direct function in heat shock gene activation [19].

We are interested in the potential involvement of JIL-1 in the process of X chromosome dosage compensation in *D. melanogaster*, which is hypothesized in light of a number of intriguing links between JIL-1 and the compensated male X chromosome. The process of dosage compensation serves to increase the transcription of genes on the single male X chromosome approximately twofold to match the combined transcription of the two alleles on the female X chromosomes [20,21]. JIL-1 is enriched on the male X chromosome and this enrichment depends on a functional DCC [2,22]. Severe reduction of JIL-1 levels leads to a global change in chromatin structure that is best appreciated on polytene chromosomes [1]. The euchromatic interbands appear much reduced in the absence of JIL-1 and replaced by atypical chromatin, in agreement with the above-mentioned role of JIL-1 in restricting the spread of heterochromatin. Interestingly, the dosage-compensated X chromosome shows an enhanced sensitivity to reduced JIL-1 levels, and appears diffuse and lacking polytene banding pattern [1,4]. The Dosage Compensation Complex (DCC, also known as Male-Specific-Lethal [MSL] complex) associates along the transcribed regions of target genes and may therefore boost transcription elongation [23,24]. The activation of genes on the male X chromosome involves the DCC subunit MOF on the X chromosome, an acetyltransferase, which selectively acetylates histone H4 at K16 (H4K16ac) [25,26]. H4K16ac opposes the folding of the nucleosomal fibre *in vitro* and should render chromatin more accessible [27]. Accordingly, chromatin from the male X chromosome is released more efficiently from nuclei after shearing [28]. However, the precise twofold enhancement of transcription cannot be explained by H4K16ac alone [26].

We now mapped for the first time at high resolution the chromosomal distribution of JIL-1 kinase in SL2 cells using chromatin immunoprecipitation (ChIP) and hybridisation of associated DNA to oligonucleotide tiling microarrays. JIL-1 binding was compared to the distribution of elongating RNA polymerase II and related to steady-state mRNA levels. We also compared them to profiles of a number of histone modifications,

and of DCC subunits. The vast majority of active genes is marked by a basal level of JIL-1 on gene bodies, independently of the actual transcription rates. The presence of H4K16ac on X-linked genes correlates with roughly twofold elevated levels of JIL-1. JIL-1 thus marks transcribed genes, but it also senses dosage-compensated chromatin. The phosphorylation of H3S10 is enriched on active genes in the same manner as JIL-1 itself. Perhaps surprisingly, the depletion of JIL-1 by RNA interference (RNAi) has only mild effects on transcription, which suggests that JIL-1 is not absolutely required for transcription in general or for dosage compensation in particular. In the light of the previous genetic analysis our data suggest that JIL contributes to a composite histone mark that may serve to reinforce the active state of chromatin by preventing the inappropriate association of silencing factors.

Results

JIL-1 binds most transcribed genes and is enriched on dosage-compensated genes

We raised two polyclonal antisera (R69 and R70) against a fragment (amino acids 79–571) of JIL-1 and established their specificity. In agreement with previous results [22], we confirmed that JIL-1 is a nuclear protein that associates with active, decondensed chromatin represented by interbands on larval polytenized chromosomes (Figure S1). We also visualized the clear enrichment of JIL-1 on the dosage-compensated, hyperactive male X chromosome. This enrichment on the X chromosomal territory can also be seen in nuclei of the *Drosophila* SL2 cells, which have a male genotype. By contrast, nuclei of female KC cells display a homogenous staining (Figure S1).

The enrichment of JIL-1 on the male X chromosome and the conflicting reports about the role of JIL-1 in the control of early transcription elongation of heat shock genes [17–19] prompted us to generate a high-resolution *in vivo* chromosomal interaction profile of the kinase and to compare it to elongating RNA polymerase II (ePol). We combined chromatin immunoprecipitation (ChIP) with probing oligonucleotide tiling arrays as before [24,26,29], using the JIL-1 antibodies and a well-established monoclonal antibody specific for ePol (H5). This antibody recognises phosphorylated serine 2 in the heptad repeat of the C-terminal domain (CTD) of the largest RNA polymerase II subunit. Data from four biological replicates starting with independent chromatin preparations were combined for each profile. The two JIL-1 antibodies gave very coherent results (Figure S2). We also generated a profile for histone H4 acetylated at K16 (H4K16ac). Figure 1 displays the profiles of JIL-1, ePol and H4K16ac along representative 250 kb portions of the chromosomes X and 3R (Figure 1A, 1B, respectively). The profiles resemble the distribution of histone H3 methylated at lysine 36 (H3K36me₃), a modification that is placed co-transcriptionally by the CTD-associated methylase Set2 and therefore serves as a hallmark of transcribed chromatin [30,31].

Qualitatively, the distribution of JIL-1 and ePol were similar on the X chromosome and on autosomes with a preference for coding sequences. In general, binding of JIL-1 to introns is lower than binding of ePol (Figure 1C). As expected, ePol is mainly found at active genes as assessed by Affymetrix expression profiling (Figure 1D) and there is a good correlation between the density of ePol along genes and the corresponding steady-state mRNA level (Figure S3). The distribution of JIL-1 correlates well with several subunits of the DCC on the X chromosome: at the probe level, the best correlations are observed with the targeting subunit MSL1 [24] and with the spreading subunit MOF, which is the

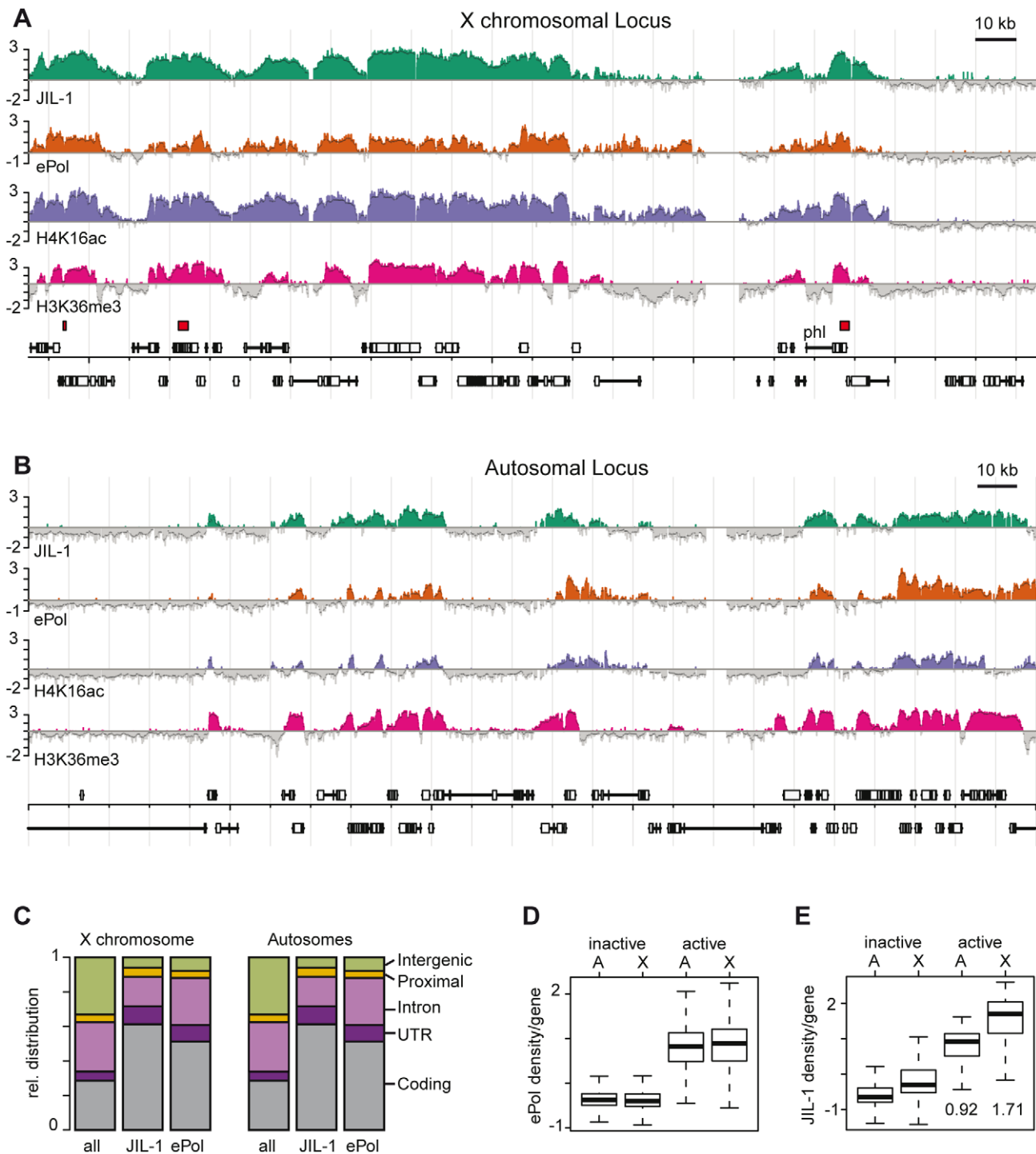


Figure 1. JIL-1 is a mark for gene activity and for dosage compensation in SL2 cells. High resolution ChIP on chip profiles of JIL-1, ePol, H4K16ac and H3K36me3 [30]. The data is represented as average log₂ signal ratio of IP over input. Bars are coloured when the signal is above zero. The dark grey line topping each profile represents the mean signal within a 500 bp window centred on the probe. High affinity sites (HAS) for the DCC according to [29] are depicted as red boxes above the gene annotations. A representative 250 kb portion has been selected (A) for the X chromosome and (B) for chromosome 3R. (C) Fractional distribution of oligonucleotides according to genomic features is shown for all probes on the array (n = 384680) and compared to the ones within JIL-1 (n = 112954) and ePol (n = 125303) binding regions as determined by hidden markov modelling. (D) The density per gene was defined as the average ratio (IP/input) of probes within a gene. The densities of ePol on autosomal genes (labelled A) and X-linked genes (labelled X) in a box plot representation. Activity status was determined by microarray expression profiling. (E) JIL-1 densities on the same sets of genes as in D, the median values for active autosomal and X-linked genes are given. The boxplot representation in all figures define 25th to 75th percentiles (boxes), 50th percentile (lines in boxes), and ranges (whiskers, 1.5 times the interquartile range extended from both ends of the box). Outliers were removed from the analysis.
doi:10.1371/journal.pgen.1001327.g001

acetyltransferase responsible for H4K16 acetylation (Figure S4). On the X chromosome 1413 genes are detectably transcribed according to ePol occupancy. Among those, the vast majority (93%) have both JIL-1 and MSL1 bound, a minority of 55 genes (4%) show no detectable JIL-1, 86 genes (6%) have no MSL1 bound, and 46 genes (3%) have neither JIL-1 nor MSL1 bound. Remarkably, the densities of ePol on active genes are comparable on autosomes and on the X chromosome (Figure 1D), although the latter ones benefit from dosage compensation (see discussion). By contrast, the mean density of JIL-1 on active genes is 0.92 for autosomal and 1.71 for X-linked genes, thus the calculated enrichment of JIL-1 on X chromosomal genes relative to autosomal ones is about 1.86 (Figure 1E). These results quantitatively reproduces the picture obtained from polytene chromosome staining (Figure S1), where a twofold enrichment had been estimated [22].

The enrichment of JIL-1 at various loci was confirmed by quantitative PCR (qPCR) on the non-amplified immunoprecipitate. Figure 2A shows as example the X chromosomal gene *pole hole* (*phl*) where JIL-1 accumulates towards the 3' end of the gene, together with H4K16ac and H3K36me3. We also confirmed the male-specific enrichment of JIL-1 on several X-linked genes by qPCR of immunoprecipitates of chromatin prepared from sorted male and female flies (Figure 2B). The X-linked genes *phl*, *CG14804*, *sta*, *Pgd* and *RpII215* show elevated levels of JIL-1 in males as compared to females. As an example for autosomal genes, we chose the *Cortactin* gene, which is similarly bound by JIL-1 in males and females. The H3K36me3 levels at the same genes are rather similar in both sexes, whereas H4K16ac is clearly found there only in males.

We conclude that JIL-1 binds active genes in both sexes and exhibits a twofold enrichment on X chromosomal genes in males.

H3 phosphorylation by JIL-1 contributes to a composite phospho-acetyl mark associated with active chromatin

In order to characterise the potential of JIL-1 to phosphorylate histones we carried out *in vitro* kinase assays using baculovirus-expressed FLAG-tagged JIL-1. Recombinant histone H3 was phosphorylated, but not histones H2A, H2B, H4 (Figure S5A). Histone H1 prepared from *Drosophila* embryos, which can be phosphorylated to some extent at serine 10 [32] was not a substrate for JIL-1 *in vitro* (not shown). We did not detect phosphorylation of H3 in nucleosomes even by increasing the salt concentration in the assay (Figure S5A). A JIL-1 derivative, in which the catalytic domain was impaired by mutating an aspartate to alanine, had no H3 kinase activity (JIL-1^{D392A}; [33]). We used H3-derived peptides to characterise the substrate specificity further and found that JIL-1 was unable to phosphorylate S28 in the context of the H3₂₁₋₃₄ peptide but efficiently phosphorylated the peptide H3₁₋₂₁. The phosphorylation occurred at serine 10 (S10) since it was abolished by incorporation of phospho-serine during peptide synthesis. At saturating amounts of peptide, neighbouring modifications of the H3 tail do not impair S10 phosphorylation (Figure S5).

H3S10 phosphorylation, particularly in the context of K14 acetylation (H3S10phK14ac) had previously been shown to be enriched on the male X chromosome [1]. By ChIP the enrichment of the straight H3S10ph epitope is difficult to document (a 1.09-fold enrichment in the data of Zhang and Oliver [28]), presumably due to the considerable amount of H3S10ph contributed by aurora kinase in mitotic cells (for review, see [34,35]). Consistent with this, JIL-1 depletion by RNAi in SL2 cells did not lead to reproducible decrease of global H3S10ph levels (Figure S6). In order to estimate the contribution of mitotic H3S10ph in

asynchronously growing SL2 cells, we arrested cells in G1/S by combined aphidicholine and hydroxyurea treatment and found the level of H3S10ph 8-fold reduced as compared to asynchronously growing cells. In the presence of the potent aurora kinase inhibitor ZM447439 [36] the global H3S10ph signal was 20 times reduced (Figure S6C). Since the proportion of mitotic SL2 cells in a culture has been estimated to be 4% [37], we conclude that the level of interphase H3S10ph is two orders of magnitude lower than that of mitotic H3S10ph. This may be an overestimate since an H3S10ph profile from ZM44743-treated cells showed very little signal over background (Figure S6E).

The detection of interphase H3S10ph in salivary glands has been shown to greatly depend on the antibody itself as well as on the procedure [19]. In particular, some antibodies may be occluded by neighbouring modifications in the H3 tail and not recognize S10ph as part of a composite epitope [38]. The two antisera used in this study, anti-H3S10ph [39] and anti-H3S10phK14ac [40] were therefore tested for their ability to recognise the S10ph mark in the presence of neighbouring modifications on the H3 tail using a custom-made peptide microarray (Figure S7). Interaction of the anti-S10ph serum, but not of the anti-S10phK14ac serum was adversely affected by the K14 acetylation. However, the latter also detected S10ph in the absence of K14 acetylation. This may explain why upon JIL-1 depletion by RNAi in SL2 cells, no decrease in H3S10phK14ac was detected by Western blotting (Figure S6D). Because the H3S10phK14ac epitope had been found enriched on the X [1] and the anti-H3S10phK14ac had been successfully used in ChIP experiments [40] we generated a global ChIP profile with the latter antibody (Figure 3A). A view of this profile along 140 kb of the X chromosome showed that H3S10phK14ac coincides with the presence of JIL-1. In addition, the H3S10phK14ac signal was enhanced on X chromosomal probes (Figure 3B) and preferentially mapped to the CDS of genes. Average binding profiles revealed that an enrichment of H3S10phK14ac throughout the transcription units can be observed in particular on X chromosomal JIL-1 target genes (Figure 3C). The global depletion of H3S10phK14ac could not be assessed by Western blot (Figure S6D), given the cross-reactivity of the antibody with (mitotic) H3S10ph but, the enrichment at the 3' end of tested target genes is reduced upon JIL-1 RNAi (Figure 3D). Taken together, the data suggest that JIL-1 contributes to generating the composite S10phK14ac modification on histone H3 at active genes.

JIL-1 increases the transcription efficiency of genes on the male X chromosome

The H3S10ph and H3S10phK14ac marks were correlated with active transcription in various model systems. In order to assess the contribution of JIL-1 to transcriptional output we reduced the levels of the kinase by RNAi in SL2 cells. Efficient depletion (up to 95%) was reproducibly achieved while ePol remained unaffected (Figure 4). This observation is in support of the results from the Johansen laboratory on salivary glands of the *JIL-1* null mutant [19]. Removal of JIL-1 did not visibly affect the association of the DCC with the X chromosomal territory, which in Figure 4C is visualised by the diagnostic H4K16ac mark. Although flies with decreasing JIL-1 levels show increasing lethality [1] the proliferation of SL2 and KC cells appears only slightly affected (proliferation was monitored for up to 19 days in RNAi conditions, not shown).

Comparison of steady-state mRNA levels in JIL-1-depleted versus control cells were assessed by Affymetrix profiling. Two sets of experiments each consisting of three biological replicates were conducted with different sets of dsRNA. The statistical analysis of

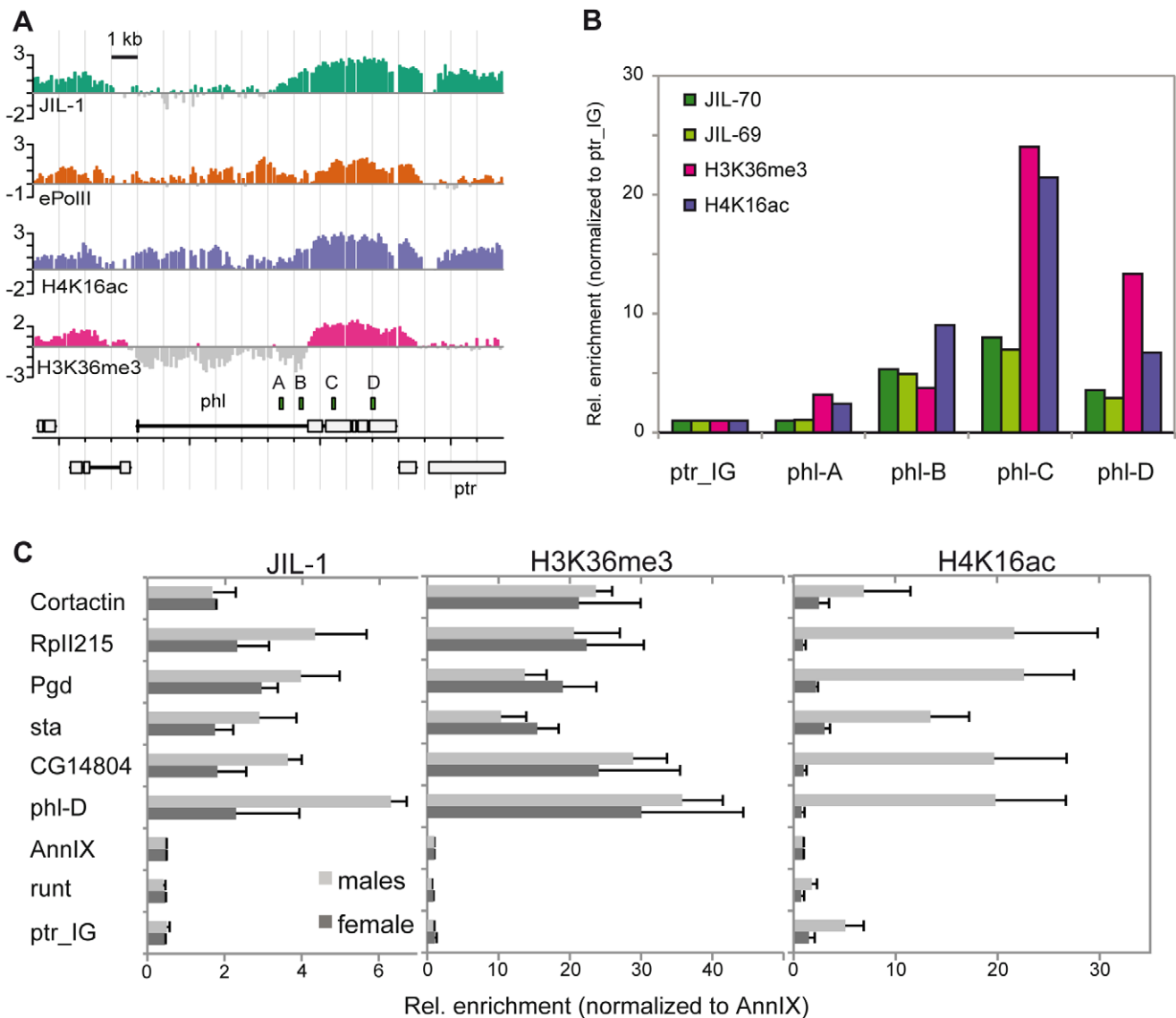


Figure 2. JIL-1 is enriched at the 3' end of *phl* and is twofold enriched at X-linked loci in male flies. Comparison of the distribution of JIL-1, ePol, H4K16ac and H3K36me3 on the X-linked gene *phl* in SL2 cells. (A) Signals as revealed by ChIP-chip profiling were compared to (B) the qPCR-based quantification of unamplified material. The position of the amplicons used for qPCR is indicated above the gene annotations. The relative enrichments from amplicons A to D were calculated using the intergenic region located ~2 kb left of the gene *ptr* (*ptr_IG*) as a reference. (C) Comparison of the enrichment of JIL-1, H3K36me3 and H4K16ac at the 3' end of the active X-linked genes *phl*, *CG14804*, *sta*, *Pgd*, *RplI215* and of the active autosomal gene *Cortactin*. The inactive X-linked gene *runt*, the promoter region of the *annexin IX* gene flanking the *Cortactin* gene and the intergenic region close to *ptr* served as negative control regions. Signals were normalized to the *annexin IX* locus and error bars represent the standard error of the mean for 3 independent biological replicates. doi:10.1371/journal.pgen.1001327.g002

effects incorporates the results of all experiments. Among several thousand active genes bound by JIL-1 in SL2 cells, we found that after JIL-1 depletion the expression level was significantly reduced for 276 genes and increased for 25 genes. Globally, transcription of X-linked genes was significantly reduced as compared to the autosomal genes (p-value $1.2e-06$) suggesting that the enrichment of JIL-1 on X-linked genes is functionally relevant for dosage compensation (Figure 4D). Interestingly, the few active genes on the fourth chromosome also appear to be particularly affected. We observed that total amount (Figure 4B) and distribution of ePol (not shown) were not changed after RNAi against JIL-1 and suggest that in SL2 cells, JIL-1 is probably not essential for the release of RNA polymerase II in productive elongation. Alterna-

tively, the few percent of JIL-1 remaining after RNAi may be sufficient to fulfil this function. It is also noteworthy that, contrary to many proteins having a function in transcriptional activation, those genes whose transcription is sensitive to JIL-1 depletion tend to have lower JIL-1 levels to start with (Figure 4E).

JIL-1 association to genes does not follow ePol

To compare the distribution of ePol and JIL-1 along genes, we scaled all genes to equal length and aligned them from transcriptional start sites (TS) to transcriptional termination sites (TT). The genes were furthermore divided into six equally sized groups based on their average ePol enrichment and average distribution profiles were computed for each group (Figure 5A

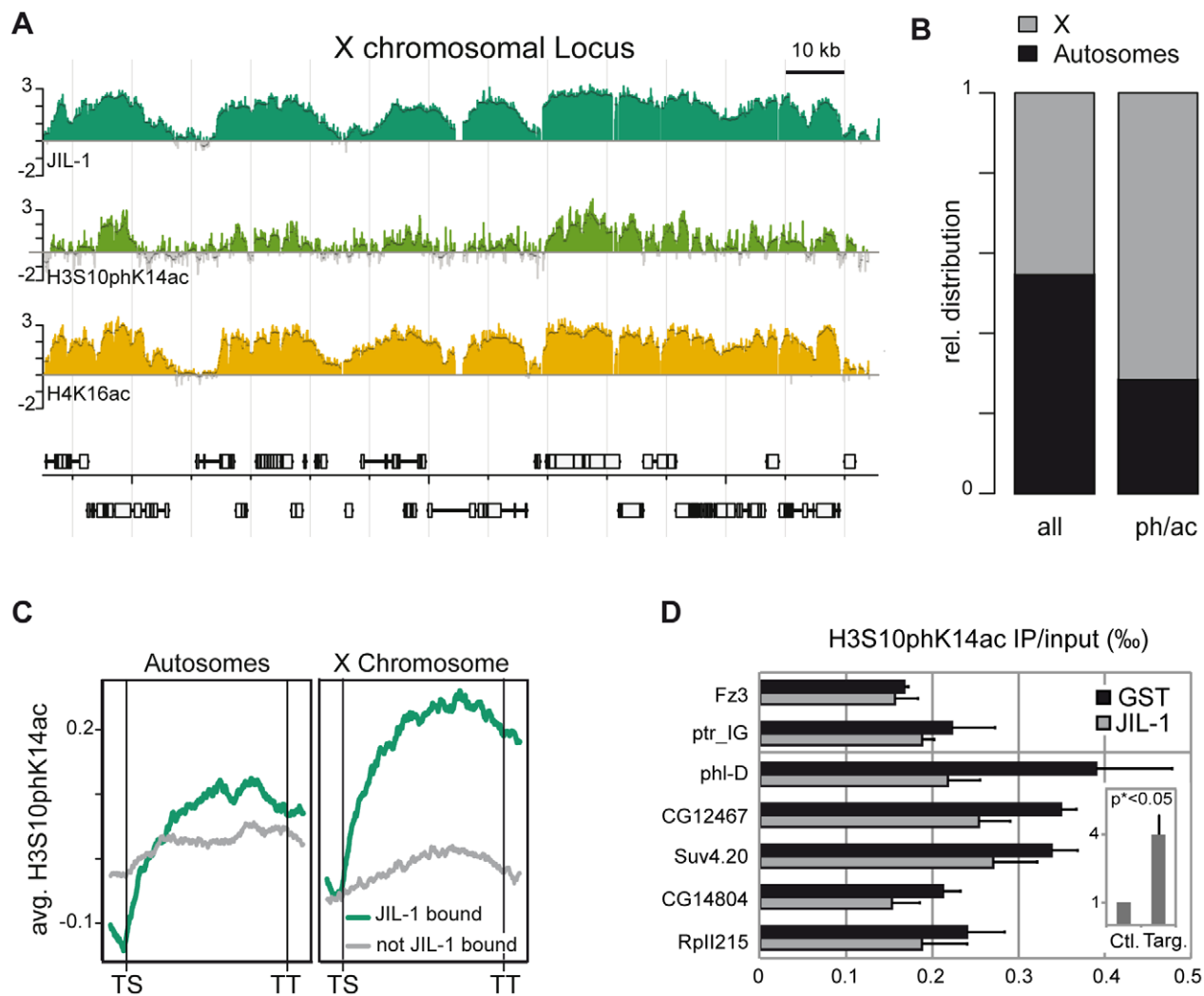


Figure 3. JIL-1-dependent H3S10phK14ac is enriched on the compensated X chromosome together with JIL-1. (A) Genome-wide distribution of H3S10phK14ac in comparison to JIL-1 and H4K16ac on a 140 kb X-chromosomal locus close to the gene *phl*. (B) Fractional distribution of probes significantly enriched for H3S10phK14ac ($n=4478$) with respect to chromosomal location. As a comparison, the distribution of all probes ($n=384680$) represented on the array is shown. (C) Cumulative binding profiles of H3S10phK14ac along genes that are either bound ($n=3362$) or not bound ($n=2050$) by JIL-1. (D) Decrease of H3S10phK14ac ChIP signal at the 3' end of the genes *phl*, *CG12467*, *Suv4.20*, *CG14804* and *Rpl1215* after JIL-1 RNAi as compared to a control GST RNAi. The intergenic region close to *ptr* and the inactive gene *Fz3* are shown as negative control regions. Results are the mean of 3 biological replicates and error bars represent the standard error of the mean. In the insert, we showed that the difference of the H3S10phK14ac ChIP signal after JIL-1 depletion is 4 times higher for target loci compared to control loci after normalization. This difference is statistically significant since the 2-sided unpaired t-test applied to the data gave a p value <0.05 . doi:10.1371/journal.pgen.1001327.g003

upper panels). The distribution of ePol along the transcribed regions is similar for autosomal and X-linked genes with a modest enrichment towards the 3' end. Monitoring the binding of JIL-1 along the gene bodies as a function of ePol density, we found that while JIL-1 clearly associated with active genes, its binding was not proportional to ePol levels (Figure 5A centre panels). Rather, three out of the four groups with significant association of ePol showed the same average binding of JIL-1, except that there was roughly twice as much JIL-1 on X-chromosomal genes compared to autosomal genes, as observed before. This property was also illustrated when the density per gene was plotted against the corresponding steady-state transcript levels. Whereas the ePol density and transcript levels correlated well, JIL-1 binding was characterized by two clouds representing autosomal and X chromosomal genes (Figure S3B). These two representations show that the density of JIL-1 on active genes is not proportional to their

transcription level. This was also observed for H3K36me3 and MSL1 distributions using the same representations (Figure S3C, S3D; Figure S8B, S8C) whereas the density of H3K4me2 and ePol were roughly proportional (Figure S8D). The discordance between ePol and JIL-1 distributions along gene bodies was even more pronounced when monitored as a function of gene length (Figure 5B). On autosomes, ePol was found enriched towards the 3' end of short genes, but for genes longer than 1.8 kb the maximal density of ePol gradually shifted towards their 5' ends as a function of length. This is also illustrated by visual inspection of very long genes both on the X and on autosomes (Figure S9). It is conceivable that the risk of premature transcription termination increases with gene length and thus leads to relative depletion of ePol at 3' ends. Interestingly, this trend was less pronounced on the X chromosome, in keeping with the attractive hypothesis that dosage compensation facilitates transcriptional elongation through

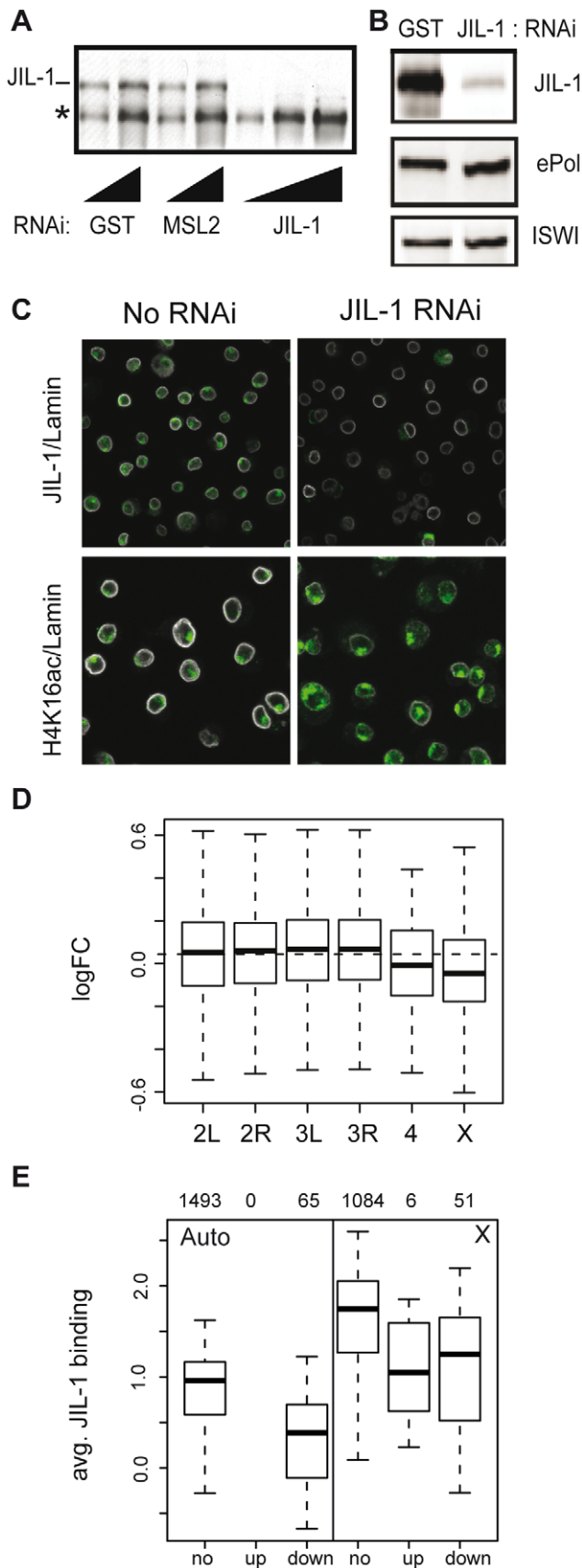


Figure 4. Effects of JIL-1 RNAi on gene expression and H4K16ac localization in SL2 cells. (A) The knock-down of JIL-1 was assessed

by western blotting on whole cell extracts after 7 days of RNA interference (RNAi). RNAi against GST and MSL2 were used as controls. The affinity-purified serum of R69 was used to detect JIL-1. A cross-reacting protein of smaller size (*) was not affected. Two and three serial dilutions of the extract were loaded for controls and JIL-1 RNAi samples, respectively. (B) Levels of ePol detected with the H5 antibody were unaffected upon JIL-1 RNAi. The ATPase ISWI served as a loading control. (C) SL2 cells were immunostained for JIL-1, H4K16ac (in green) and lamin (in white) and analyzed by confocal imaging. (D) Log₂ fold changes in gene expression after JIL-1 RNAi as compared to GST or GFP RNAi (ctr RNAi) summarized by chromosomes in a box plot. The dashed horizontal line indicates the median change of all active genes. (E) The average binding of JIL-1 per gene was plotted for autosomal genes on the left (Auto) and X-linked genes on the right (X) distinguishing genes with no expression change over JIL-1 depletion ('no'), up-regulated genes ('up') and down-regulated genes ('down'). The numbers on top indicate the number of genes in each category. doi:10.1371/journal.pgen.1001327.g004

chromatin. By contrast, the relative distribution of JIL-1 along genes of various lengths is comparable on autosomes and the X chromosome, except for the twofold enrichment on the latter (Figure 5B).

JIL-1 recruitment upon gene activation

A recent suggestion that JIL-1-dependent H3S10 phosphorylation was crucial to regulate the release of RNA polymerase into productive elongation in *Drosophila* in particular for the transcription of heat shock genes has remained controversial [17–19]. In our hands, heat shock treatment for 2, 5 and 10 min in SL2 cells triggered a clear enrichment of ePol at the *Hsp70* locus as monitored by ChIP without strikingly affecting the distribution of JIL-1. In particular, we found that there was already some ePol and some JIL-1 at that locus in control cells as evidenced by the comparison with the active X-linked locus *sta* (Figure S10). Western blotting showed that the overall level of ePol drops upon heat shock, whereas the levels of JIL-1 varied only slightly. Because heat shock had been shown to trigger a massive loss of nucleosomes over a large domain [41], and because the genome-wide localization of JIL-1 appeared to correlate best with histone modifications (see below), we speculate that the lack of recruitment might be a consequence of nucleosome depletion.

We next made use of an inducible reporter system in flies ([26,42]; Figure 6A), which harbours an insertion of a reporter gene cassette consisting of the *lacZ* gene downstream of five binding sites for the yeast transcription factor Gal4 ('upstream activating sequences'; UAS_{Gal}). The reporter was activated by crossing the reporter fly line with a line expressing either Gal4 alone or MOF fused to the Gal4 DNA binding domain (Gal4_{DBD}). The basal level of β-galactosidase expression in the absence of activation was very low and could be induced about 1000-fold in male and female flies by expression of Gal4 under the control of a tubulin promoter. We monitored the levels of JIL-1, H3K36me3 and H4K16ac at the 5' and 3' ends of the *lacZ* gene by ChIP. As reference for the normalisation of the ChIP signals from different chromatin preparations we used the intergenic locus close to *ptr* (*ptr_IG*). In accordance with the results presented in Figure 2C, the X-chromosomal gene *phl* showed robust enrichment of JIL-1 in female flies and approximately twofold elevated levels in males. Very little recruitment of JIL-1 was observed at the reporter gene upon activation via Gal4 (Figure 6B). However, we did also not detect robust levels of H3K36me3 as compared to the endogenous loci. Since the tubulin-Gal4 driver leads to strong activation, which can be visualized by clear puffing at the level of polytene chromosomes, it is possible that these histone marks have been depleted along with nucleosomes due to vigorous transcription, a

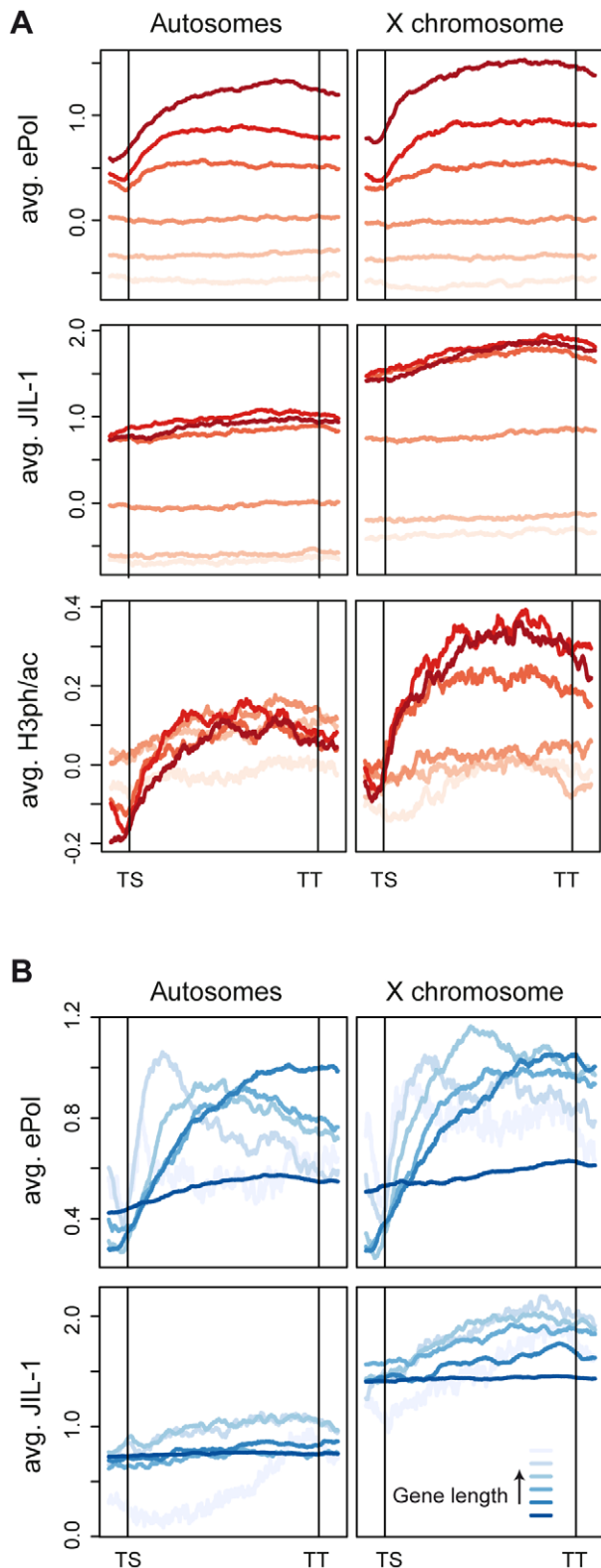


Figure 5. JIL-1 distributes differently than elongating polymerase on active chromatin. Average distribution profiles of chromatin features along genes scaled for length from transcription start (TS) to termination sites (TT). (A) All genes covered by the tiling array were grouped into 6 equally-sized bins based on increasing densities of ePol. Average profiles of ePol (top), JIL-1 (centre) and H3S10phK14ac (bottom) were calculated for each group. The increasing darkness of the red lines indicate an increasing density of ePol on the

genes between the groups. (B) Genes were binned based on their length. The length distribution within the bins is the following: 287-1204, 1204-1780, 1780-2477, 2477-3778, 3778-7400 and 7400-162904 bp. Average profiles on the grouped genes are displayed for ePol (top) and JIL-1 (bottom).
doi:10.1371/journal.pgen.1001327.g005

situation akin to the heat-induced transcription mentioned earlier. In order to trigger a more modest induction of the reporter gene we expressed the acetyltransferase MOF fused to the Gal4_{DBD} (Gal4-MOF) at a low level from its endogenous promoter [26]. We limited this analysis to females in order to avoid the complications associated with all other members of the DCC. We had shown earlier that recruitment of Gal4-MOF to the reporter locus in females leads to H4K16ac and to a substantial transcriptional activation [26]. In the current experiment the activation was determined to be about 20-fold in the β -galactosidase assay. This activation was accompanied by an enrichment of JIL-1 at the 3' end of the *lacZ* reporter (13-fold over the intergenic locus *ptr_IG*), which was about twofold higher than the enrichment at the endogenous X-linked locus *phl* (Figure 6C). In this case of a mild activation, we found an enrichment of H3K36me3 at the 3' of the *LacZ* reporter, which was comparable to the endogenous loci *phl* and *Cortactin*. Upon induction with MOF, a 7-fold enrichment of H4K16ac is detected at the 5' end of the *LacZ* reporter, which decreased towards the 3' end. The *Cortactin* gene, localised about 2-3 kb downstream of the UAS_{GAL} as mapped by PCR-rescue of the transgene, also showed an increased level of H4K16ac upon Gal4-MOF targeting. Interestingly, the presence of H4K16ac in addition to H3K36me3 on the reporter gene *LacZ* correlated with an enrichment of JIL-1 comparable to that of X-linked genes in males. On the neighbouring *Cortactin* gene the enrichment was also increased. We found that the enrichment of both H4K16ac and JIL-1 at the *Cortactin* gene only increased the expression of the gene by a factor 1.2 in females. In accordance with previous data [26], in males H4K16ac spreads out more broadly from the recruitment sites due to the presence of the DCC and the relative expression of the *Cortactin* gene was increased by a factor 1.6 (Figure S11). Taken together the recruitment experiments suggest that the association of JIL-1 with active genes rather correlates with the presence of H3K36me3 and H4K16ac than with transcription as such. This conclusion can be substantiated by visual inspection of the genome-wide ChIP-chip profiles from SL2 cells, where numerous instances can be found where JIL-1 binding closely parallels the presence of H3K36me3, whereas the presence of high levels of ePol alone and sometimes also significant enrichment of H4K16ac alone do not coincide with JIL-1 binding (see Figure S9 for a selection of views).

JIL-1 recruitment and dosage compensation

In order to further explore the relationship between JIL-1, transcription, H3K36me3 and H4K16ac, we looked in more detail at the relative twofold enrichment of JIL-1 on the male X chromosome. Johansen and colleagues [22] had documented earlier that the enrichment of JIL-1 on the male X chromosome depends on the DCC. Their key experiment was the ectopic expression of MSL2 in female larvae, which leads to inappropriate assembly of the DCC. The association of the DCC with the female X chromosome led to an enrichment of JIL-1, just like in males [22]. In agreement with these data, in similar experiments we found that if high levels of MSL2 are expressed from two NOPU alleles [43,44] the X chromosome is decorated with DCC and JIL-1 is enriched concomitantly at sites of DCC binding. However,

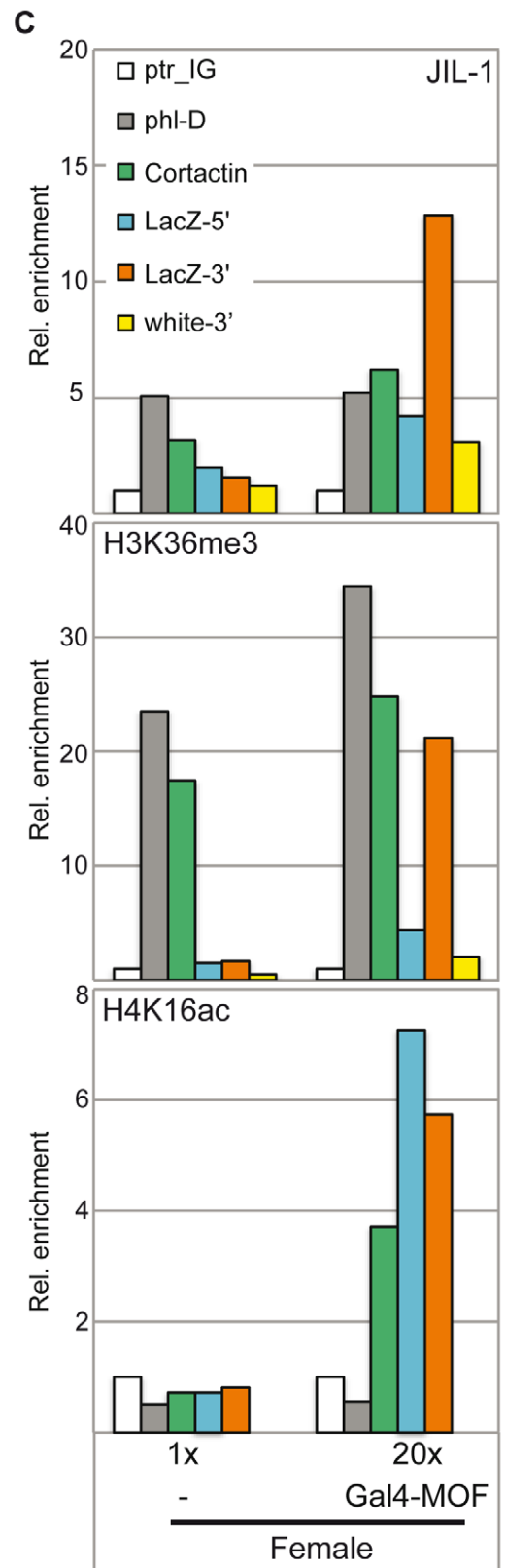
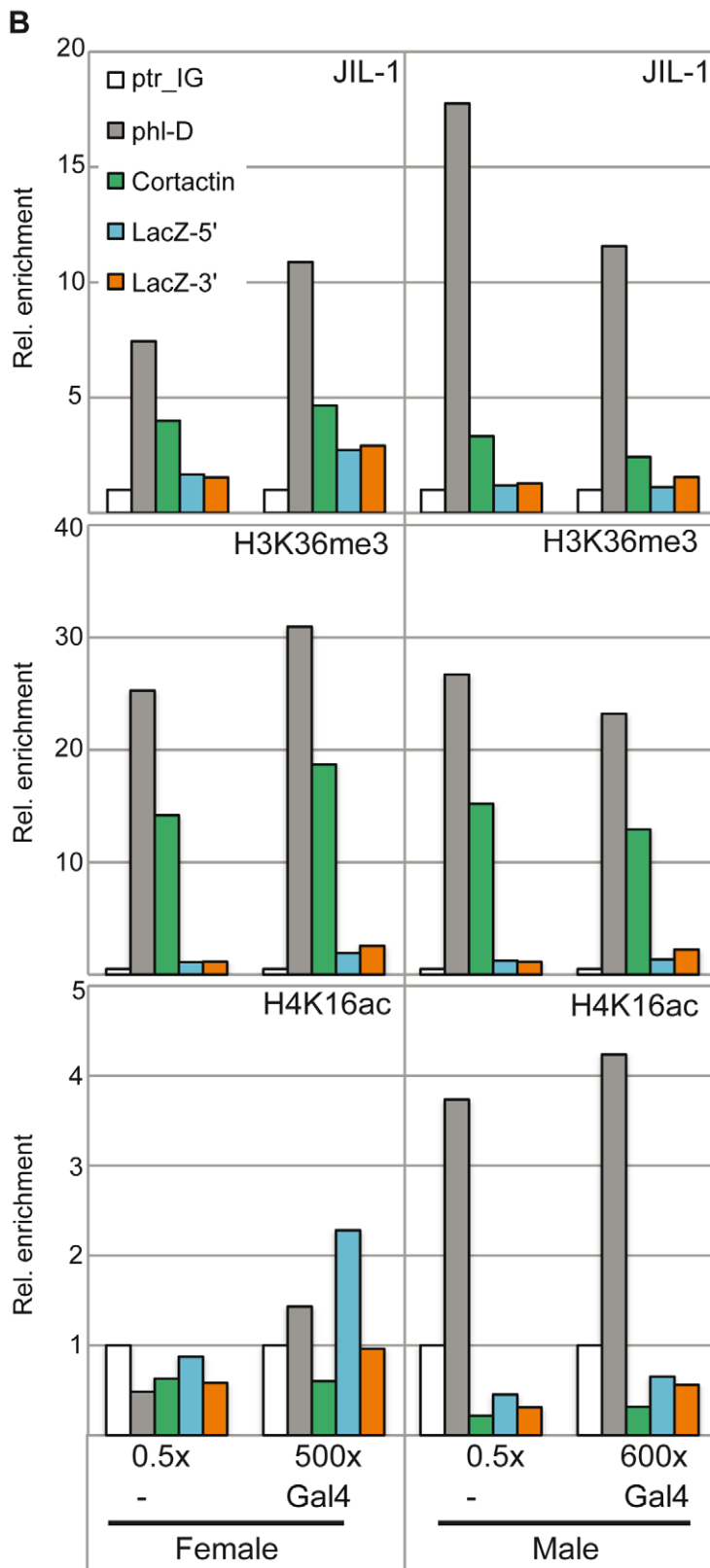
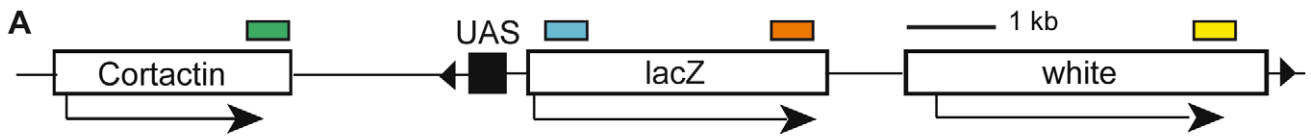


Figure 6. JIL-1 distribution upon activation of a reporter construct in flies. (A) The reporter construct encompassing five UAS in front of a *LacZ* reporter carries a *miniwhite* gene [42]. It is inserted on 3R at position 93B8 with the UAS close to the 3' end of the *Cortactin* gene. The cartoon is drawn to scale, except for the negligible size of the UAS in order to visualize the distances between the amplicons (coloured boxes) used for qPCR analysis in panels B and C. (B) Activation of the *LacZ* reporter was achieved by crossing the homozygote reporter line to the *Tubulin-Gal4/TM3* driver line expressing Gal4_{fl} under control of the *tubulin* promoter. Relative β -galactosidase activity as measured in the corresponding flies is provided on the bottom of the panels. The reference was set to 0.5 \times for the heterozygote reporter line in the absence of activation. The ChIP signals for JIL-1 (upper panel), H3K36me3 (centre panel) and H4K16a (lower panel) at the intergenic locus (*ptr_IG*), at the 3' of active X-linked gene (*phl-D*), at the 3' of the *Cortactin* gene and at the 5' and 3' of the *LacZ* reporter gene are displayed. The data is provided as relative enrichments over the intergenic locus (*ptr_IG*). (C) For activation of the reporter by Gal4-MOF, the homozygote reporter line was used as a reference and compared to the stable line carrying both the homozygote reporter construct and the homozygote transgene leading to Gal4-MOF expression [26]. Only females were analyzed. The activity measurements for the two different types of females are mentioned below the graphs and can be compared to the values in B. In addition to the amplicons used in (B) we also analyzed binding to the 3' end of the *miniwhite* gene. Because of the inherent variability of chromatin preparation one representative biological replicate is presented here.

doi:10.1371/journal.pgen.1001327.g006

when limiting levels of MSL2 are expressed from the *SXB1-2* allele [43,44] the DCC only associates with about 50 high affinity sites (HAS) on polytene chromosomes. In this case, the enrichment of JIL-1 can only be seen at sites of DCC binding (Figure 7A). This enrichment requires the assembly of a complete DCC, including MOF, as it is not observed in the absence of MLE or MSL3 ([22] and data not shown).

The close relationship between DCC association and JIL-1 was also apparent at the high resolution achieved by ChIP-chip mapping. We had earlier identified 131 HAS that are preferentially bound by limiting amounts of DCC [29]. Plotting the binding of MSL1 to genes as a function of their distance to the closest HAS shows that, in general, the closer a gene resides to a HAS, the more MSL1 and H4K16ac can be found (Figure 7B). The same trend can be observed for JIL-1 as well as for the linked H3S10phK14ac mark: their densities are decreasing with increasing distance to a HAS. This is, however, not true for H3K36me3 or ePol association (Figure 7B).

In summary, diverse experiments establish two hallmarks of active chromatin that correlate with the presence of JIL-1. First, there is an excellent correlation of JIL-1 binding to H3K36me3-marked chromatin. On top of this basal level of binding, the presence of the DCC leads to an approximately twofold enrichment of JIL-1. Indeed, a global comparison of ChIP-chip probe signals (Figure 8) reveals that the correlations of JIL-1 signals with the ones of H3K36me3 ($R = 0.758$) or H4K16ac ($R = 0.76$) are very good. Remarkably, the combination of both marks (sum of the intensities of the H3K36me3 and H4K16ac signals) correlated even better with JIL-1 signals ($R = 0.899$) and displayed an almost linear relationship between signal intensities. This is true if all probes are considered, but also if autosomal or X chromosomal probes are plotted separately (Figure 8). This correlation can be recapitulated to some extent when the distribution of those marks is considered along genes (Figure S12). In contrast, correlation of JIL-1 and ePol ($R = 0.69$) is less pronounced (Figure 8). This result is consistent with the earlier observation that ePol and JIL-1 are both marks for active genes but that their relative distributions along genes differ (Figure 5).

We conclude that two distinct targeting principles that are represented by H3K36me3 and H4K16ac marks determine the level of JIL-1 recruitment to active genes.

Discussion

Targeting of JIL-1

The genome-wide mapping of JIL-1 and ePol in male SL2 cells together with the reporter assay in flies suggest that JIL-1 is part of a network of factors that collectively define the state of active chromatin. Taken together with previous genetic analyses, our data lead us to consider to a role for JIL-1 not in the establishment

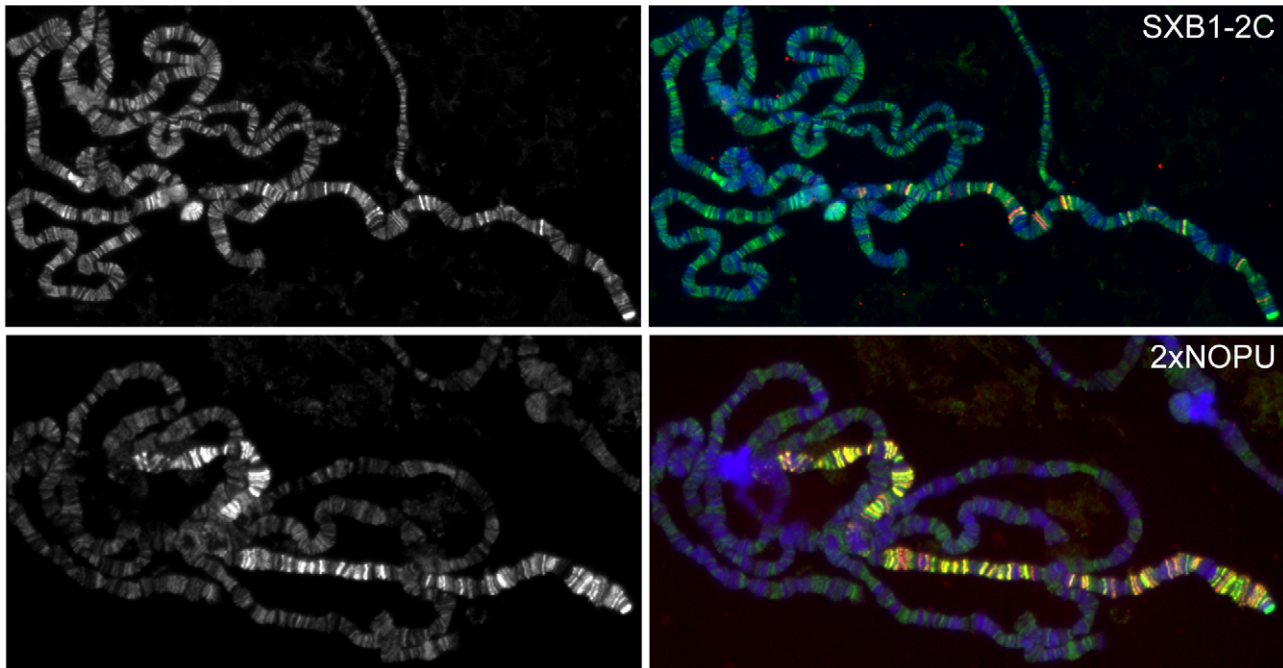
of active chromatin, but in the reinforcement of the active state, independently of the extend of transcription.

Although JIL-1 binds the bodies of most active gene and is recruited to a reporter gene upon activation, the degree of binding does not correlate well with ePol occupancy. In this respect JIL-1 belongs to a class of several other active chromatin components whose presence in chromatin does not scale with ePol, such as H3K36me3, the DCC subunit MSL1, or H4K16ac mark. By contrast, H3K4me2 levels are proportional to ePol levels. Conceivably, JIL-1 marks active chromatin independent of whether it is currently transcribed or not. A basal level of JIL-1 binding correlates strongly with H3K36me3, an elongation marker that is placed co-transcriptionally by ePol-associated dSet2 [30]. The turnover time of this modification is not known and hence it is possible that H3K36me3 remains on chromatin between pulses of transcription.

Most recently, high-resolution mapping of 56 chromatin components using Dam-ID revealed five types of chromatin in *Drosophila* KC cells [45]. A colour code was used to illustrate those types. The two types of active chromatin, 'red' and 'yellow', differ in that active genes in red chromatin tend to be depleted in H3K36me3 and MRG15, which are abundant constituents of yellow chromatin. Monitoring the relative distributions of ePol and JIL-1 in those types of chromatin we found that whereas ePol is equally distributed in red and yellow chromatin, JIL-1 is clearly mostly found in yellow chromatin (Figure S13). This correlation again highlights the relationship between JIL-1 and H3K36me3. The precise link between H3K36me3 and JIL-1 recruitment remains to be explored (see below).

A second targeting principle is evident from the fact that JIL-1 levels are approximately twofold increased on the male X chromosome, where due to the action of the DCC H4K16ac levels are high. The situation is complex since the recruitment of the DCC to transcribed genes on the X chromosome is promoted by the potential interaction of the DCC subunit MSL3 with H3K36me3 [30]. Because JIL-1 binding is insensitive to different transcription rates on autosomes, it is not plausible that a presumed twofold increase in transcription on the X chromosome is directly responsible for this elevated association. Likewise, we do not think that direct interactions between JIL-1 and the DCC can explain the targeting. Although some interactions have been observed *in vitro* between JIL-1, MSL1 and MSL3 [22], a quantitative co-purification of endogenous JIL-1 with the DCC was never documented. Indeed, activation of a reporter gene in female flies through recruitment of Gal4-MOF is sufficient to recruit JIL-1 to male levels on the reporter gene and on the adjacent *Cortactin* gene. Altogether, we favour the hypothesis that the enrichment of JIL-1 on X-linked genes is a consequence of a modulating feature of dosage-compensated chromatin. The genome-wide distribution of JIL-1 indeed correlates best with the combination of the two chromatin modifications, H3K36me3

A



B

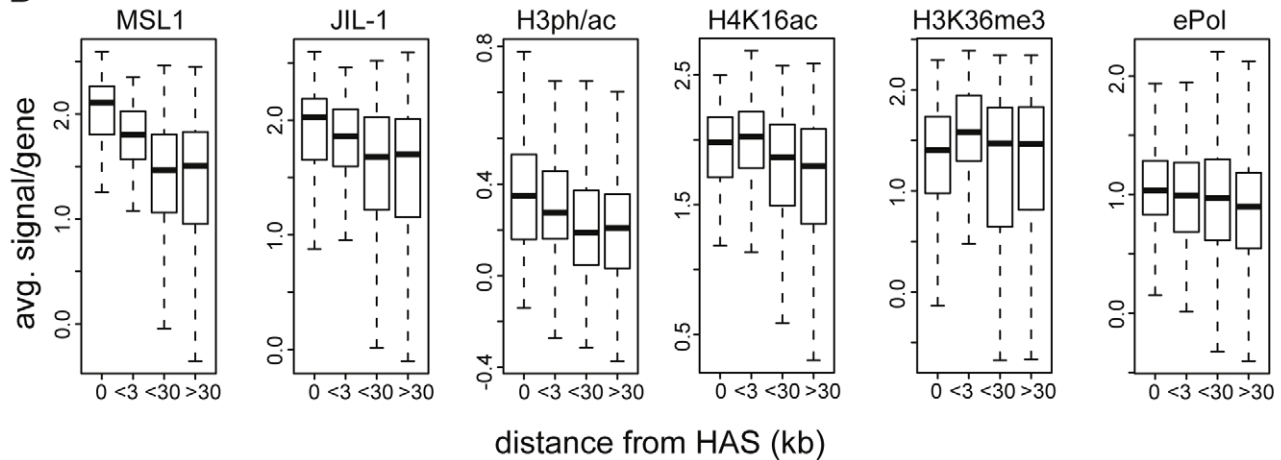


Figure 7. Distribution of JIL-1 on the X-chromosome. (A) Localization of JIL-1 (left panels, green in the merged pictures) in SXB1-2C and 2xNOPU females expressing increasing amounts of MSL2 (coloured red in the merged pictures on the right). (B) Densities of various features on active X-chromosomal genes grouped by increasing distance from high affinity sites (HAS) for the DCC. There are 115, 121, 405 and 465 genes in the group of genes located at increasing distances from HAS, respectively.
doi:10.1371/journal.pgen.1001327.g007

and H4K16ac, on the X-chromosome suggesting that JIL-1 recruitment occurs downstream of those two histone marks. Interestingly, the correlation still holds for autosomal probes, although autosomal H4K16ac is at least in part placed at the 5' end of genes by alternative MOF complexes [26,46,47]. JIL-1 recruitment has also been linked to the H4K12ac mark, which is placed by the GCN5-containing ATAC complex [48]. However, Workman and colleagues recently found that ATAC also contains an acetyltransferase with specificity for H4K16 (atac2), which may contribute to JIL-1 recruitment [49].

In the cases of very strong transcription activation by high levels of Gal4 activator, we did not see an accumulation of JIL-1 to endogenous levels. Conversely, JIL-1 is also not enriched at

developmental puffs on polytene chromosomes where robust transcription takes place according to the strong ePol staining (Figure S1). The massive heat-induced activation leads to extensive chromatin decondensation (puffing) on polytene chromosomes, which is probably accompanied by nucleosome loss [41].

In summary, we favour the idea that the recruitment of JIL-1 relies on several, partly redundant features of active chromatin. JIL-1 harbours an H3-tail binding domain in its C-terminus and another determinant of chromatin targeting in its N-terminal domain [3], but it does not contain any domain known to directly bind modified histone tails. Its recruitment to active chromatin is, therefore, most probably indirect. We know of no histone modification or any other chromatin-associated feature to be enriched on the male X

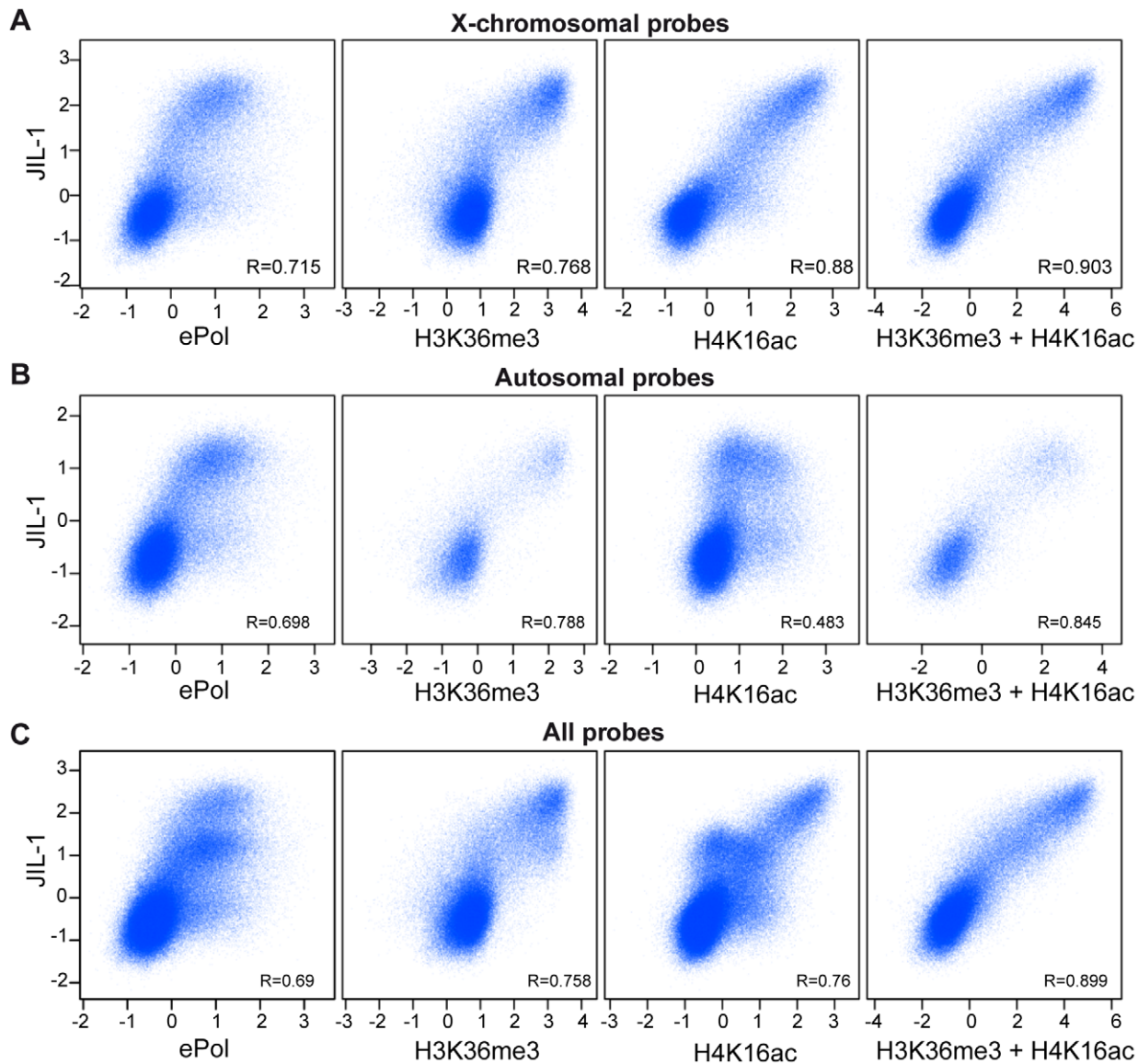


Figure 8. Correlations of H3K36me3, H4K16ac, and JIL-1 binding. Pair-wise correlations of JIL-1 versus ePol, H3K36me3, H4K16ac and the sum of H3K36me3 and H4K16ac signals in unified 200 bp sampling windows. (A) Results for the X chromosome (B) for autosomes (C) and for the entire genome. Pearson correlation coefficients are provided for each panel. doi:10.1371/journal.pgen.1001327.g008

chromosome except for JIL-1 and the JIL-1-dependent phosphoacetyl mark. An appealing model for JIL-1 targeting is that its general recruitment mode (correlating with H3K36me3) would be the same on all chromosomes. The additional presence of H4K16ac might enhance the access of JIL-1 to the first targeting principle, since it has been shown that H4K16ac prevents the folding of the nucleosomal fibre into more compact structures [27].

Effects of H3S10 phosphorylation by JIL-1

It has been observed that histone H3S10ph can enhance acetylation of histone H3K14 [50,51] and inhibit methylation of histone H3K9 [52]. The biochemical analysis of JIL-1 kinase showed that a number of other modifications of the H3 N-terminus are compatible with the phosphorylation by JIL-1. Therefore, JIL-1 phosphorylation is compatible with the prior existence of other modifications, consistent with a downstream function of JIL-1.

Our data suggest that in *Drosophila* the function of H3S10ph may at least in part differ from that in other organisms, where it is implicated in the fast and transient induction of promoters in response to various inducers [13,16,53,54]. In *Drosophila*, JIL-1 is not particularly enriched at promoters, but associates with genes along their entire length. This distribution is more compatible with a role in fine-tuning transcriptional elongation. The effects of JIL-1 may – at least in part – be mediated by 14-3-3 proteins, which are able to recognize the interphase H3S10ph mark [17,54].

The depletion of JIL-1 has a clear but small effect on overall transcription. The fact that JIL-1 binds gene bodies rather than promoters and the binding is independent of actual transcription rates leads us to speculate that the kinase may influence transcription efficiency only very indirectly by reinforcing the active chromatin state – once established by co-activators – by protecting it from neighbouring repressive chromatin. This could become important when moderately active genes are not

constantly transcribed. Highly transcribed genes experience nucleosome depletion and therefore do not provide anchoring sites for silencing factors. Moderately transcribed genes, however, may experience periods without active elongation [55–57]. These ‘gaps’ bear the risk of placement of silencing marks, most notable H3K9me2. In this context JIL-1 may safeguard active genes (marked by H3K36me3 as a sign of recent transcriptional activity). This function may be achieved by phosphorylation of H3S10, which prevents the recognition of HP1 by occlusion of H3K9me2 [58,59] but possibly also by phosphorylation of other substrates, like Su(var)3,9 [33]. In addition JIL-1 might have a scaffolding function for other factors, like lamins [60]. The observation that genes sensitive to the depletion of JIL-1 tend to have less JIL-1 bound both on the X chromosome and on autosomes also support a model where JIL-1 is associated to active chromatin domains to prevent the spreading of more repressive structures. We speculate that the role of JIL-1 in maintaining the balance between heterochromatin and euchromatin is not only true at the hetero/euchromatin boundary, but also within euchromatin at the level of active chromatin domains.

Materials and Methods

JIL-1 antibodies and kinase assay

Polyclonal antisera were raised in two rabbits against a fragment of JIL-1 corresponding to amino acids 79–571, which was expressed in fusion with an N-terminal MBP-tag in *E. coli* (Eurogentec). The resulting sera R69 and R70 were either used crude or after affinity purification on a column with covalently coupled antigen according to a standard protocol. For Western blot, the sera were diluted 1/2000 and affinity-purified antibodies were used at 0.5 µg/ml. Recombinant Flag-tagged JIL-1 and kinase assay conditions were as previously described [33].

Reporter lines and β-galactosidase activity measurements

The transgenic line used for the reporter assay in flies was originally published as U/15 [42]. The P-element insertion site was mapped by PCR-rescue to the 3′ end of the *Contextin* gene (Figure 6A). To activate the reporter by the Gal4 activator homozygote flies of the reporter line were crossed with males of the activator line, which carry a transgene driving the expression of the Gal4 activator under the control of the *tubulin* promoter (Bloomington Stock Center #5138). Gal4 is expressed from the cellular blastoderm onwards. The F1 flies were hand-sorted according to their genotype and sex in order to obtain 190–250 mg of flies for chromatin preparation. β-galactosidase activity in extracts prepared from 2–10 flies were measured as previously described [26]. The flies carrying the balancer were used as negative controls for the flies carrying the Gal4 activator. To activate the reporter by Gal4-MOF recruitment, we used a stable line homozygote for the reporter construct and prepared chromatin for ChIP from sorted 200–500 female flies [26].

Chromatin immunoprecipitation

Chromatin from SL2 cells was prepared after crosslinking in 1% formaldehyde as previously described [29]. To preserve the phospho-epitopes and the acetylation status of the chromatin, we used 5 mM NaF, 20 mM β-glycerophosphate, 0.1 mM NaVanadate, 10 mM NaButyrate and a mixture of protease inhibitors (1mM PMSF, 1 µg/ml of each aprotinin, pepstatin and leupeptin) or the complete protease inhibitors (Roche, Cat No. 04693132011). In the particular case of the chromatin used for mapping H3S10phK14ac, 1 µM microcystin was also added.

The chromatin from sorted male and/or female flies was done according to following references [26,61]. Chromatin shearing to 300–1000 bp fragments was assessed on a Bioanalyzer (Agilent) and DNA concentration was measured using NanoDrop (Thermo Scientific). 7.5 to 10 µg of DNA per chromatin was used for ChIP. For JIL-1 ChIPs we used either crude sera R69 and R70 (5 µl/IP) or the affinity-purified antibodies (5 µg/IP). A LiCl wash was done for ChIP-chip analysis. For ePol ChIPs, 5 µl of the anti-CTD S2ph monoclonal antibody Cone H5 (ab24758, Abcam) was first coupled to a 50/50 mix of protein A- and protein G-agarose using a bridging antibody (5 µg of Goat anti-mouse IgM, Jackson ImmunoResearch) and the LiCl wash was omitted. The following volumina of antibodies were used for ChIP: H3S10phK14ac: 3 µl; H4K16ac: 5 µl of antibody #39167 (Active Motif); H3K36me3: 5 µl of ab9050 (Abcam). MSL2 antibodies were used as control as previously published [62].

Quantitative PCR

Quantitative PCR (qPCR) was carried out in an ABI PRISM 7000 Sequence detection system in a 25 µl reaction with Power SYBR Green Master Mix (Applied Biosystems) or in LightCycler (Roche) in 10 µl reactions with Fast SYBR Green Master mix (Applied Biosystems). Input DNA were diluted to 10 ng/µl and ChIPs were diluted 1/30, 5 µl and 2 µl template were used for ABI PRISM 7000 and LightCycler, respectively. The results were comparable on the two machines. Primer sequences are provided in Table S1.

ChIP-chip and data analysis

ChIP-chip data analysis was essentially performed as in [29]. Briefly, input and IP DNA were amplified using the WGA kit (Sigma) according to the online protocol (<http://www.epigenome-noe.net/WWW/researchtools/protocol.php?protid=30>). Labeling and hybridization to NimbleGen dual-color arrays was carried out at ImaGenes (Berlin, Germany). The layout of the array (approx. 1 probe/100 bases, isothermal probe design) was customized [24]. Data analysis was performed using R/Bioconductor (www.bioconductor.org). Experimental replication was as follows: JIL-1: 4 biological replicates; H3S10phK14ac: 2 biological replicates including dye swap; elongating RNA Polymerase II: 3 biological replicates including one dye swap; H4K16ac: 2 biological replicates including dye swap. Raw signals of corresponding biological samples were log2 transformed and quantile-normalized. Enrichment statistics (IP versus input signals) were computed using the ‘sam’ algorithm within Bioconductor [63]. Fdr values of the sam statistic were determined using ‘locfdr’ [64] region summarization was performed using tileHMM [65] with the following parameters: fragment size of 700, maximal gap of 400. Genes were considered ‘bound’ if covered by at least 4 probes with a posterior probability above 0.5. All data correspond to *Drosophila* genome version dm3 and annotation version gadfly 5.2.2.

RNAi in SL2 cells and purification of total RNA

SL2 cells were cultured according to standard methods. RNA interference (RNAi) was carried out as published [66] except that 2×10^6 cells were treated with 10 µg dsRNA and splitted 1/3 after 3 days of treatment. After 7 days cells were collected and counted prior to total RNA purification. For the 2 sets of expression analysis we used different sets of dsRNA for RNAi. In experiment 1, the 5′ coding sequence of JIL-1 was targeted by a corresponding dsRNA (T7_JIL-15′_for: TTAATACGACTCACTATAGGGGATGAGTCGCTTG, T7_JIL-15′_rev: TTAATACGACTCACTATAGGGGAGACATCCTCCTCCA), and the controls involved treating cells with dsRNA targeting GST sequences

(T7_GST_for: TTAATACGACTCACTATAGGGAGAATGTCCCCTATACTAGGTTA, T7_GST_rev: TTAATACGACTCACTATAGGGAGAACGCATCCAGGCATTG). In the second set JIL-1 was knock-down by targeting its 3' coding sequences (T7_JIL-13'_for: TTAATACGACTCACTATAGGGAGACAGCAGCGTCG, T7_JIL-13'_rev: TTAATACGACTCACTATAGGGAGATTGGAAGTGTAT) and the control dsRNAs represented GFP sequences (T7_GFP_for: TTAATACGACTCACTATAGGGTGTGCTCAGGTAGTGGTTGTCG, T7_GFP_rev: TTAATACGACTCACTATAGGGCCTGAAAGTTCATCTGCACCA). Off-target effects were minimized using <http://dscheck.rnai.jp/>. Efficiency of the depletion was assessed on whole cell extracts and quantified with the Odyssey imaging system (LI-COR, Biosciences) using anti-tubulin (T9026, clone DM1A, Sigma) or anti-lamin (Clone T40, [67]) as reference. Total RNA was purified from $20\text{--}80 \times 10^6$ cells using either the RNA purification kit (RNeasy mini kit, Qiagen) or the lysis reagent (Qiazol, Qiagen) according to manufacturers instructions. The quality of the RNA was determined on the Bioanalyzer (Agilent).

Expression analysis after JIL-1 RNAi

Total RNA was processed for hybridization at ImaGenes (Berlin, Germany). Five biological replicates for each control and JIL-1 RNAi were analysed. Microarray data were processed using R/Bioconductor (www.bioconductor.org). Unless indicated otherwise we used standard parameters in all function calls. Expression values were calculated using 'gcRMA'. Probe sets were kept for differential expression analysis if there were more 'present' calls (calculated using 'mas5calls') in one of the two treatment groups than non-'present' calls and if their expression level variance was higher than 0 across all arrays. "One gene to many probe set" relationships were resolved by retaining only the probe set with the highest variance across all arrays. Differential expression statistics were obtained using a linear model (library 'limma') including a batch effect coefficient as two sets of arrays were processed at different times. A significant response was defined if the local false discovery ('locfdr' package) rate calculated on the moderated t statistic was smaller than 0.2.

Microscopy

Polytene chromosome staining was according to [44]. The affinity-purified antibodies R70 or R69 were used diluted 1/150 and the H5 monoclonal antibody at 1/50. Staining of SL2 cells was according to a standard protocol. In brief, after fixation with 3.7% (w/v) formaldehyde in PBS buffer, the cells were permeabilised with 0.3% triton X-100 (v/v) in PBS in the presence of 1% formaldehyde. The affinity-purified antibodies of R70 or R69 were diluted at 0.4 µg/ml, the anti-H4K16ac antibody #39167 (ACTIVE MOTIF) was diluted 1/1000 for counterstaining of the X-chromosome territory, and the anti-lamin clone T40 [67] was diluted at 1/100 to delimitate the nuclear territory. Epifluorescence microscopy was done on the Axiovert 200 inverted microscope (Zeiss) and confocal images were taken using LSM510 Meta system (Zeiss).

Accession numbers

Microarray data has been deposited at GEO (accession GSE22620). The Nimblegen tiling data have been deposited at GEO (accession GSE22618).

Supporting Information

Figure S1 Quality control of the JIL-1 antibodies in western blot and immunostaining. (A) Equivalent loading of SL2 whole cell

extract (lane 1), Soluble fraction (lane 2) and Chromatin fraction (lane 3) were probed in western blot detection for JIL-1 (R70), tubulin (Tub) and histone H3. JIL-1 is enriched in the chromatin fraction. The asterisk marks a cross-reacting protein detected by R70 affinity purified antibodies, which is mostly in the cytoplasmic fraction. Coomassie staining of the fractions is shown below. M: Molecular weight markers. (B) Staining of male and female wt polytene chromosomes with anti-JIL-1 serum R70 and with the H5 mAb against ePol. For accurate comparison a male and a female salivary gland were processed together on one slide. On the left are the chromosomes of a female nucleus and on the right the chromosomes of a male nucleus. (C) Staining of *Drosophila* cells. In female KC cells JIL-1 (probed with R69) is evenly distributed in the nucleus. The hyperactivated X chromosome is detected by MSL3 staining in the male SL2 cells. JIL-1 enrichment on the X chromosome territory is observed with the two different affinity-purified antibodies R69 and R70 both used at 0.4 µg/ml. Found at: doi:10.1371/journal.pgen.1001327.s001 (3.55 MB TIF)

Figure S2 Quality control of JIL-1 antibodies in ChIP. (A) The two affinity-purified antibodies raised against JIL-1 were used for ChIP-on-Chip from one batch of SL2 chromatin. A 250 kb portion of the X chromosome around *phi* for the two antibodies R69 and R70 is shown. (B) Corresponding correlation plot for the two independent profiles gives a Pearson correlation coefficient of $R = 0.89$.

Found at: doi:10.1371/journal.pgen.1001327.s002 (1.17 MB TIF)

Figure S3 JIL-1, H3K36me3, and MSL1 densities on genes are not proportional to transcript level. (A) Scatter plot representation illustrating the correlation of the steady-state mRNA levels determined on Affymetrix expression arrays (x axis) and the density of various features on genes (y axis). The Pearson correlation coefficients are given for each plot. Average density of ePol per gene. (B) Average density of JIL-1 per gene. (C) Average density of H3K36me3 per gene [30]. (D) Average density of MSL1 per gene [24].

Found at: doi:10.1371/journal.pgen.1001327.s003 (3.32 MB TIF)

Figure S4 Comparison of ePol, JIL-1, and DCC subunits distributions on the X Chromosome. (A) Distributions of JIL-1, ePol, MSL1, MSL2, MSL3 [23] and MOF are shown on a 250 kb portion of the X chromosome. (B) Correlation plots of the different data sets.

Found at: doi:10.1371/journal.pgen.1001327.s004 (2.67 MB TIF)

Figure S5 JIL-1 kinase activity on histone H3 peptides, histone octamers, and oligo-nucleosomes. (A) Kinase assays of recombinant Flag-JIL-1 on recombinant histone H3 and H3 peptides harbouring various modifications have been analyzed by SDS-PAGE and autoradiography. The quantification on 3 independent replicate assays is represented on the left and one of the autoradiogram on the right. (B) Autoradiogram of a kinase assay with 2 µg of reconstituted recombinant histone octamers on the left and 2 µg of the same octamers assembled on a plasmid DNA to oligo-nucleosomes. Titration of increasing concentration of NaCl in the assays showed that the activity of JIL-1 (autophosphorylation and H3 phosphorylation in octamers) slightly drops but does not favour the phosphorylation of H3 within oligo-nucleosomes.

Found at: doi:10.1371/journal.pgen.1001327.s005 (1.21 MB TIF)

Figure S6 Contribution of mitotic and interphase H3S10ph in SL2 cells. (A) Western blot quantification of H3S10ph after JIL-1 (J1, J2, J3) and control GST RNAi (G1, G2, G3) in SL2 cells in 3 independent replicate experiments. After titration experiments with SL2 cells as well as with the derived clones L2.4 (kind gift of

Dr. P. Heun, MPI for Immunology, Freiburg, Germany) and SF4 (kind gift of D. Arndt-Jovin, MPI for Biophysical Chemistry, Göttingen, Germany), we found that Sf4 cells showed the best response and remained healthy under the various treatment conditions. (B) FACS analysis of asynchronously growing SF4 cells (in green, labelled As), SF4 cells arrested at in G1/S after treatment for 16 hours with aphidicholin (10 μ M) and hydroxyurea (1.5 mM) (in red, labelled A/H), and SF4 cells treated with the aurora kinase inhibitor ZM44739 (50 μ M) for 16 hours (in blue, labelled ZM). (C) Western blot quantification of H3S10ph in SF4 cells arrested in G1/S (A/H) and treated with aurora kinase inhibitor (ZM). (D) Western blot quantification of H3S10phK14ac after JIL-1 RNAi in asynchronous and G1/S arrested L2.4 cells. (E) Comparison of the high resolution ChIP on chip profile of H3S10phK14ac presented in Figure 3 with H3S10ph profiles obtained from A/H treated cells and from ZM treated cells. A 250 kb portion of the X chromosome is shown. Found at: doi:10.1371/journal.pgen.1001327.s006 (1.44 MB TIF)

Figure S7 Specificities of the anti-histone H3 tail antibodies used in this study. Peptide chips (JPT Peptide Technology) consisting of three replicate arrays of 158 peptides, mostly histone peptides furnished with known posttranslational modifications or combination of modifications have been used to test the selectivity of (A) the anti-H3S10phK14ac serum [40], (B) the anti-H3S10ph serum and (C) the same anti-H3S10ph antibodies after affinity purification [39]. All of them were incubated in PBS, 3% BSA at 1/10,000 dilution. A secondary antibody coupled to an IR dye was then used for detection with the Odyssey system (LI-COR Biosciences). The strongest reactivity seen for the H4(86-98) peptide in panel C is due to the secondary antibody. The insert in each panel shows the mean signal for each spotted peptide in the three replicated arrays. Found at: doi:10.1371/journal.pgen.1001327.s007 (1.64 MB TIF)

Figure S8 Comparison of the gene-wise distribution of various features for genes of increasing ePol density. (A) Same representation as in Figure 5 with 6 groups of genes of increasing ePol density for both autosomes and X chromosome. (B) Average distribution of H3K36me3 for the groups of genes defined in A. (C) Average distribution of MSL1. (D) Average distribution of H3K4me2. Found at: doi:10.1371/journal.pgen.1001327.s008 (0.96 MB TIF)

Figure S9 JIL-1 and H3K36me3 distribution on long genes. (A) Five active autosomal genes and (B) 5 active X-linked genes are depicted using the same colour code and scales as in Figure 1. The strong similarity of the distribution of JIL-1 (green) and H3K36me3 (pink) on long genes in SL2 cells is illustrated. Those genes often have a long 5' intron, which is decorated by ePol (orange) and H4K16ac (blue) but depleted in H3K36me3 and JIL-1. Found at: doi:10.1371/journal.pgen.1001327.s009 (2.30 MB TIF)

Figure S10 ePol and JIL-1 distribution in SL2 cells upon heat shock treatment. SL2 cells were subjected to 2', 5' and 10' heat shock treatment as previously described [68] and processed for ChIP according to our standard protocol. Chromatin from uninduced (NHS) cells was used as a reference. The primers for

qPCR analysis are as described [68]. (A) ePol ChIP. (B) JIL-1 ChIP. (C) Western blot quantification of ePol, JIL-1 and H3K36me3 in the different chromatin preparation.

Found at: doi:10.1371/journal.pgen.1001327.s010 (1.16 MB TIF)

Figure S11 *Cortactin* expression upon Gal4-mof recruitment in the reporter lines. Total RNA was prepared from sorted males and females of the reporter line and of the line with additional expression of Gal4-mof. Quantitative RT-PCR was done to evaluate the expression of the *Cortactin* gene relative to that of the housekeeping gene *Tub97E*. The mean of 3 measurements on different cDNA dilutions is represented and error bars are the standard error of the mean. The corresponding relative enrichment of H4K16ac at the *Cortactin* gene in ChIP experiments is mentioned below the graph.

Found at: doi:10.1371/journal.pgen.1001327.s011 (0.49 MB TIF)

Figure S12 JIL-1 distribution along genes scales with H3K36me3 and H4K16ac. Average distribution profiles of chromatin features along genes scaled for length from transcription start (TS) to termination sites (TT). The JIL-1 distribution is shown for all genes covered on both our tiling array and the tiling array used for H3K36me3 profiles [30] after grouping into six equally-sized bins (containing about 455 genes each) for both autosomal and X-linked probes separately based on (A) increasing densities of H3K36me3, (B) increasing density of H4K16ac and (C) increasing density of H3K36me3+H4K16ac.

Found at: doi:10.1371/journal.pgen.1001327.s012 (0.46 MB TIF)

Figure S13 ePol and JIL-1 partition differentially in various chromatin types. (A) Partitioning of ePol in the five chromatin types [45]. (B) Partitioning of JIL-1 in the five types of chromatin. (C) Relative distribution of all probes in the five types of chromatin is compared to ePol and JIL-1 enriched probes. (D) A 180 kb portion of the X chromosome is shown where ePol and JIL-1 mark a green chromatin domain together with H3K9me2. (E) A 180 kb portion of an autosome is shown to illustrate the colocalisation of JIL-1, H3K36me3 and MRG15 colocalize in yellow chromatin.

Found at: doi:10.1371/journal.pgen.1001327.s013 (1.12 MB TIF)

Table S1 List of qPCR primer sequences used in this work.

Found at: doi:10.1371/journal.pgen.1001327.s014 (0.03 MB PDF)

Acknowledgments

We thank M. Prestel for the reporter fly line expressing Gal4-Mof, C. Grimaud for mapping the insertion of the transgene of the reporter fly line, H. Mitlöchner for fly pushing, and M. Prestel and R. Villa for critical reading of the manuscript. We are grateful to C. Seiser for the anti-H3S10phK14ac serum, to L. Mahadevan for the anti-H3S10ph serum, to M. Kuroda for the anti-MSL3 serum, and to H. Saumweber for the T40 anti-lamin antibody.

Author Contributions

Conceived and designed the experiments: CR PBB. Performed the experiments: CR AM IKD VF. Analyzed the data: CR TS. Wrote the paper: CR TS PBB.

References

- Wang Y, Zhang W, Jin Y, Johansen J, Johansen KM (2001) The JIL-1 tandem kinase mediates histone H3 phosphorylation and is required for maintenance of chromatin structure in *Drosophila*. *Cell* 105: 433–443.
- Jin Y, Wang Y, Walker DL, Dong H, Conley C, et al. (1999) JIL-1: a novel chromosomal tandem kinase implicated in transcriptional regulation in *Drosophila*. *Mol Cell* 4: 129–135.
- Bao X, Cai W, Deng H, Zhang W, Krencik R, et al. (2008) The COOH-terminal domain of the JIL-1 histone H3S10 kinase interacts with histone H3 and is required for correct targeting to chromatin. *J Biol Chem* 283: 32741–32750.
- Deng H, Zhang W, Bao X, Martin JN, Girton J, et al. (2005) The JIL-1 kinase regulates the structure of *Drosophila* polytene chromosomes. *Chromosoma* 114: 173–182.

5. Deng H, Bao X, Cai W, Blacketer MJ, Belmont AS, et al. (2008) Ectopic histone H3S10 phosphorylation causes chromatin structure remodeling in *Drosophila*. *Development* 135: 699–705.
6. Zhang W, Deng H, Bao X, Lerach S, Girton J, et al. (2006) The JIL-1 histone H3S10 kinase regulates dimethyl H3K9 modifications and heterochromatic spreading in *Drosophila*. *Development* 133: 229–235.
7. Lerach S, Zhang W, Bao X, Deng H, Girton J, et al. (2006) Loss-of-function alleles of the JIL-1 kinase are strong suppressors of position effect variegation of the *wm4* allele in *Drosophila*. *Genetics* 173: 2403–2406.
8. Bao X, Deng H, Johansen J, Girton J, Johansen KM (2007) Loss-of-function alleles of the JIL-1 histone H3S10 kinase enhance position-effect variegation at pericentric sites in *Drosophila* heterochromatin. *Genetics* 176: 1355–1358.
9. Ebert A, Schotta G, Lein S, Kubicek S, Krauss V, et al. (2004) Su(var) genes regulate the balance between euchromatin and heterochromatin in *Drosophila*. *Genes Dev* 18: 2973–2983.
10. Deng H, Bao X, Zhang W, Girton J, Johansen J, et al. (2007) Reduced levels of Su(var)3-9 but not Su(var)2-5 (HP1) counteract the effects on chromatin structure and viability in loss-of-function mutants of the JIL-1 histone H3S10 kinase. *Genetics* 177: 79–87.
11. Deng H, Cai W, Wang C, Lerach S, Delattre M, et al. (2010) JIL-1 AND SU(VAR)3-7 Interact Genetically and Counteract Each Other's Effect on Position Effect Variegation in *Drosophila*. *Genetics*.
12. Vermeylen L, Berghe WV, Beck IM, De Bosscher K, Haegeman G (2009) The versatile role of MSKs in transcriptional regulation. *Trends Biochem Sci* 34: 311–318.
13. Winter S, Simboeck E, Fischle W, Zupkovitz G, Dohal I, et al. (2008) 14-3-3 proteins recognize a histone code at histone H3 and are required for transcriptional activation. *EMBO J* 27: 88–99.
14. Vicent GP, Ballare C, Nacht AS, Clausell J, Subtil-Rodriguez A, et al. (2006) Induction of progesterone target genes requires activation of Erk and Msk kinases and phosphorylation of histone H3. *Mol Cell* 24: 367–381.
15. Macdonald N, Welburn JP, Noble ME, Nguyen A, Yaffe MB, et al. (2005) Molecular basis for the recognition of phosphorylated and phosphoacetylated histone h3 by 14-3-3. *Mol Cell* 20: 199–211.
16. Zippo A, Serafini R, Rochigiani M, Pennacchini S, Krepelova A, et al. (2009) Histone crosstalk between H3S10ph and H4K16ac generates a histone code that mediates transcription elongation. *Cell* 138: 1122–1136.
17. Karam CS, Kellner WA, Takenaka N, Clemmons AW, Corces VG (2010) 14-3-3 Mediates Histone Cross-Talk during Transcription Elongation in *Drosophila*. *PLoS Genet* 6: e1000975. doi:10.1371/journal.pgen.1000975.
18. Ivaldi MS, Karam CS, Corces VG (2007) Phosphorylation of histone H3 at Ser10 facilitates RNA polymerase II release from promoter-proximal pausing in *Drosophila*. *Genes Dev* 21: 2818–2831.
19. Cai W, Bao X, Deng H, Jin Y, Girton J, et al. (2008) RNA polymerase II-mediated transcription at active loci does not require histone H3S10 phosphorylation in *Drosophila*. *Development* 135: 2917–2925.
20. Straub T, Becker PB (2007) Dosage compensation: the beginning and end of generalization. *Nat Rev Genet* 8: 47–57.
21. Gelbart ME, Kuroda MI (2009) *Drosophila* dosage compensation: a complex voyage to the X chromosome. *Development* 136: 1399–1410.
22. Jin Y, Wang Y, Johansen J, Johansen KM (2000) JIL-1, a chromosomal kinase implicated in regulation of chromatin structure, associates with the male specific lethal (MSL) dosage compensation complex. *J Cell Biol* 149: 1005–1010.
23. Alekseyenko AA, Larschan E, Lai WR, Park PJ, Kuroda MI (2006) High-resolution ChIP-chip analysis reveals that the *Drosophila* MSL complex selectively identifies active genes on the male X chromosome. *Genes Dev* 20: 848–857.
24. Gilfillan GD, Straub T, de Wit E, Greil F, Lamm R, et al. (2006) Chromosome-wide gene-specific targeting of the *Drosophila* dosage compensation complex. *Genes Dev* 20: 858–870.
25. Gelbart ME, Larschan E, Peng S, Park PJ, Kuroda MI (2009) *Drosophila* MSL complex globally acetylates H4K16 on the male X chromosome for dosage compensation. *Nat Struct Mol Biol* 16: 825–832.
26. Prestel M, Feller C, Straub T, Mitlöchner H, Becker PB (2010) The activation potential of MOF is constrained for dosage compensation. *Molecular Cell* 38: 815–826.
27. Shogren-Knaak M, Ishii H, Sun JM, Pazin MJ, Davie JR, et al. (2006) Histone H4-K16 acetylation controls chromatin structure and protein interactions. *Science* 311: 844–847.
28. Zhang Y, Oliver B (2010) An evolutionary consequence of dosage compensation on *Drosophila melanogaster* female X-chromatin structure? *BMC Genomics* 11: 6.
29. Straub T, Grimaud C, Gilfillan GD, Mitterweger A, Becker PB (2008) The chromosomal high-affinity binding sites for the *Drosophila* dosage compensation complex. *PLoS Genet* 4: e1000302. doi:10.1371/journal.pgen.1000302.
30. Larschan E, Alekseyenko AA, Gortchakov AA, Peng S, Li B, et al. (2007) MSL complex is attracted to genes marked by H3K36 trimethylation using a sequence-independent mechanism. *Mol Cell* 28: 121–133.
31. Lee JS, Shilatufard A (2007) A site to remember: H3K36 methylation a mark for histone deacetylation. *Mutat Res* 618: 130–134.
32. Villar-Garea A, Imhof A (2008) Fine mapping of posttranslational modifications of the linker histone H1 from *Drosophila melanogaster*. *PLoS ONE* 3: e1553. doi:10.1371/journal.pone.0001553.
33. Boeke J, Regnard C, Cai W, Johansen J, Johansen KM, et al. (2010) Phosphorylation of SU(VAR)3-9 by the chromosomal kinase JIL-1. *PLoS ONE* 5: e10042. doi:10.1371/journal.pone.0010042.
34. Giet R, Glover DM (2001) *Drosophila aurora B* kinase is required for histone H3 phosphorylation and condensin recruitment during chromosome condensation and to organize the central spindle during cytokinesis. *J Cell Biol* 152: 669–682.
35. Nowak SJ, Corces VG (2004) Phosphorylation of histone H3: a balancing act between chromosome condensation and transcriptional activation. *Trends Genet* 20: 214–220.
36. Gadea BB, Ruderman JV (2005) Aurora kinase inhibitor ZM447439 blocks chromosome-induced spindle assembly, the completion of chromosome condensation, and the establishment of the spindle integrity checkpoint in *Xenopus* egg extracts. *Mol Biol Cell* 16: 1305–1318.
37. Morales-Mulia S, Scholey JM (2005) Spindle pole organization in *Drosophila* S2 cells by dynein, abnormal spindle protein (Asp), and KLP10A. *Mol Biol Cell* 16: 3176–3186.
38. Clayton AL, Hazzalin CA, Mahadevan LC (2006) Enhanced histone acetylation and transcription: a dynamic perspective. *Mol Cell* 23: 289–296.
39. Clayton AL, Rose S, Barratt MJ, Mahadevan LC (2000) Phosphoacetylation of histone H3 on c-fos- and c-jun-associated nucleosomes upon gene activation. *EMBO J* 19: 3714–3726.
40. Brunmeir R, Lagger S, Simboeck E, Sawicka A, Egger G, et al. (2010) Epigenetic regulation of a murine retrotransposon by a dual histone modification mark. *PLoS Genet* 6: e1000927. doi:10.1371/journal.pgen.1000927.
41. Petesch SJ, Lis JT (2008) Rapid, transcription-independent loss of nucleosomes over a large chromatin domain at Hsp70 loci. *Cell* 134: 74–84.
42. Zink D, Paro R (1995) *Drosophila* Polycomb-group regulated chromatin inhibits the accessibility of a trans-activator to its target DNA. *EMBO J* 14: 5660–5671.
43. Kelley RL, Wang J, Bell L, Kuroda MI (1997) Sex lethal controls dosage compensation in *Drosophila* by a non-splicing mechanism. *Nature* 387: 195–199.
44. Dahlsven IK, Gilfillan GD, Shelest VI, Lamm R, Becker PB (2006) Targeting determinants of dosage compensation in *Drosophila*. *PLoS Genet* 2: e5. doi:10.1371/journal.pgen.0020005.
45. Filion GJ, van Bemmel JG, Braunschweig U, Talhout W, Kind J, et al. (2010) Systematic protein location mapping reveals five principal chromatin types in *Drosophila* cells. *Cell* 143: 212–224.
46. Kind J, Vaquerizas JM, Gebhardt P, Gentzel M, Luscombe NM, et al. (2008) Genome-wide analysis reveals MOF as a key regulator of dosage compensation and gene expression in *Drosophila*. *Cell* 133: 813–828.
47. Raja SJ, Charapitsa I, Conrad T, Vaquerizas JM, Gebhardt P, et al. (2010) The nonspecific lethal complex is a transcriptional regulator in *Drosophila*. *Molecular Cell* 38: 827–841.
48. Ciurciu A, Komonyi O, Boros IM (2008) Loss of ATAC-specific acetylation of histone H4 at Lys12 reduces binding of JIL-1 to chromatin and phosphorylation of histone H3 at Ser10. *J Cell Sci* 121: 3366–3372.
49. Suganuma T, Gutierrez JL, Li B, Florens L, Swanson SK, et al. (2008) ATAC is a double histone acetyltransferase complex that stimulates nucleosome sliding. *Nat Struct Mol Biol* 15: 364–372.
50. Lo WS, Trievel RC, Rojas JR, Duggan L, Hsu JY, et al. (2000) Phosphorylation of serine 10 in histone H3 is functionally linked in vitro and in vivo to Gen5-mediated acetylation at lysine 14. *Mol Cell* 5: 917–926.
51. Cheung P, Tanner KG, Cheung WL, Sassone-Corsi P, Denu JM, et al. (2000) Synergistic coupling of histone H3 phosphorylation and acetylation in response to epidermal growth factor stimulation. *Mol Cell* 5: 905–915.
52. Rea S, Eisenhaber F, O'Carroll D, Strahl BD, Sun ZW, et al. (2000) Regulation of chromatin structure by site-specific histone H3 methyltransferases. *Nature* 406: 593–599.
53. Zippo A, De Robertis A, Serafini R, Oliviero S (2007) PIM1-dependent phosphorylation of histone H3 at serine 10 is required for MYC-dependent transcriptional activation and oncogenic transformation. *Nat Cell Biol* 9: 932–944.
54. Winter S, Fischle W, Seiser C (2008) Modulation of 14-3-3 interaction with phosphorylated histone H3 by combinatorial modification patterns. *Cell Cycle* 7: 1336–1342.
55. Fuda NJ, Ardehali MB, Lis JT (2009) Defining mechanisms that regulate RNA polymerase II transcription in vivo. *Nature* 461: 186–192.
56. Hager GL, McNally JG, Misteli T (2009) Transcription dynamics. *Mol Cell* 35: 741–753.
57. Wijgerde M, Grosveld F, Fraser P (1995) Transcription complex stability and chromatin dynamics in vivo. *Nature* 377: 209–213.
58. Fischle W, Tseng BS, Dormann HL, Ueberheide BM, Garcia BA, et al. (2005) Regulation of HP1-chromatin binding by histone H3 methylation and phosphorylation. *Nature* 438: 1116–1122.
59. Hirota T, Lipp JJ, Toh BH, Peters JM (2005) Histone H3 serine 10 phosphorylation by Aurora B causes HP1 dissociation from heterochromatin. *Nature* 438: 1176–1180.
60. Bao X, Zhang W, Krencik R, Deng H, Wang Y, et al. (2005) The JIL-1 kinase interacts with lamin Dm0 and regulates nuclear lamina morphology of *Drosophila* nurse cells. *J Cell Sci* 118: 5079–5087.
61. Negre N, Hennequin J, Sun LV, Lavrov S, Bellis M, et al. (2006) Chromosomal distribution of PcG proteins during *Drosophila* development. *PLoS Biol* 4: e170. doi:10.1371/journal.pbio.0040170.

62. Gilfillan GD, Konig C, Dahlsveen IK, Prakoura N, Straub T, et al. (2007) Cumulative contributions of weak DNA determinants to targeting the *Drosophila* dosage compensation complex. *Nucleic Acids Res* 35: 3561–3572.
63. Tusher VG, Tibshirani R, Chu G (2001) Significance analysis of microarrays applied to the ionizing radiation response. *Proc Natl Acad Sci U S A* 98: 5116–5121.
64. Efron B (2007) Correlation and large scale simultaneous significance testing. *Jour Amer Stat Assoc* 102: 99–103.
65. Humburg P, Bulger D, Stone G (2008) Parameter estimation for robust HMM analysis of ChIP-chip data. *BMC Bioinformatics* 9: 343.
66. Straub T, Neumann MF, Prestel M, Kremmer E, Kaether C, et al. (2005) Stable chromosomal association of MSL2 defines a dosage-compensated nuclear compartment. *Chromosoma* 114: 352–364.
67. Risau W, Saumweber H, Symmons P (1981) Monoclonal antibodies against a nuclear membrane protein of *Drosophila*. Localization by indirect immunofluorescence and detection of antigen using a new protein blotting procedure. *Exp Cell Res* 133: 47–54.
68. Boehm AK, Saunders A, Werner J, Lis JT (2003) Transcription factor and polymerase recruitment, modification, and movement on dhsp70 in vivo in the minutes following heat shock. *Mol Cell Biol* 23: 7628–7637.